Investigating Black Hole Kicks

Serena Repetto

Lund Observatory
Lund University

2011-EXA52

Degree project of 30 higher education credits (for a degree of Master)
April 2011

Lund Observatory
Box 43
SE-221 00 Lund
Sweden

Investigating Black Hole Kicks

Serena Repetto

May 6, 2011

Abstract

It has been known for some time that neutron stars receive kicks (so-called natal kicks) when they are formed in core-collapse supernovae. Whether black holes receive these kicks too is still a matter of debate. We study Galactic low-mass X-ray binaries containing a black hole as the accreting object and look at their position within the Galaxy: some systems are almost coplanar, while others are found in the halo. Starting from sensible guesses on the initial binary properties and assuming the objects to be originated in the plane of the Galaxy, we perform a series of Monte Carlo simulations in which we calculate the trajectories of low-mass X-ray binary systems that receive a kick when the progenitor of the black hole explodes as a supernova, and determine their resulting location in the Galaxy. The comparison between the simulated distribution and the observed one leads us to conclude that a natal kick is indeed required for the formation of the systems.

We shall not cease from exploration
And the end of all our exploring
Will be to arrive where we started
And know the place for the first time.
T.S. Eliot

Contents

Acknowledgements

I arrived here in Lund Observatory last October. From the very first moment, I had the impression that there was something special about this Department: I immediately felt comfortable and surrounded by cheerful and dynamic people. Doing science is also made by the people you work with and here in Lund there's always something to learn or to be curios about, while discussing with people at the traditional coffee breaks or after one of the seminars. I firmly believe that ideas become more powerful when shared and shaped from different point of views: this never lacks in Lund Observatory.

First, I want to thank Melvyn Davies, for giving me the opportunity of working on such an interesting and profound topic. The project was concrete while doing it, as well as concrete are the results. Working with Melvyn helped me realize how important is the balance between hard work and creative inspiration. I learnt and grew a lot as an astrophysicist while discussing with him: his guesses and new ideas always led me to re-evaluate things, never taking them for granted.

I would like to thank all people in Astro, students, professors, technical staff, for making me feel always welcomed. My Erasmus could not have been better and this is thanks to all of you.

Masters and PhDs, of course: our parties are always the best. Thank you for making my weekends here in Sweden always full of events: no time for getting bored with you!

My office mates, David O. and Adrian. David, our discussion on science were always inspiring and your cutting-edge music selection while working late, really priceless. Adrian, your open-minded and positive mood always greeted me entering the office. Thank you, guys!

My lovely friends Chiara and Erica, for always cheering me up, for our girlish nights, for all the very emotional moments and for "putizza", of course.

And, Alexey: thank you for all the support, the laughts, the rush biking trips and for coming up with crazy and unconventional ideas, always.

I will never forget my Swedish life.

1 Introduction

Since black holes don't emit visible radiation, we have to look for indirect ways of investigating their formation scenario.
X-ray binaries, in particular, harbor a wealth of information on how black holes are formed. They allow us to *measure* natal kicks, i.e. the velocities that a compact object might receive at birth due to asymmetries in the supernova event.

X-ray binaries containing a neutron star as the compact object have been largely investigated in the past. The more systematic analysis is the one done by Brandt & Podsiadlowski [6]: they study the effects of high supernova kick velocities on the orbital parameters of neutron-star binaries, both in the case of low-mass companion (LMXB) and in the case of high-mass companion (HMXB). Their LMXBs simulations highlight the consistency of the observed Galactic distribution with a normal Galactic disc population that has been widened because of significant kick the systems received at birth. This result is consistent with the measured high space velocities of radio pulsars. Instead, HMXBs tend to be much more coplanar, because of their younger age, and because of the lower kicks received at birth.

Assuming that black holes are born in the same way as neutron stars, that is in core-collapse supernovae, one legitimate question is whether they suffer of kicks comparable to the ones typical of neutron stars. The investigation of the kick distribution is important since it affects our interpretation of the space distribution of black-hole candidates in the Milky Way (in particular of their Galactic scale height) as well as our understanding of how black holes are formed.

2 Generalities on binary systems

2.1 The two-body problem

About half of all stars in the Milky Way are found in systems consisting of two or more stars, the so called *binary* (or multiple) *stellar systems*. Stellar binary systems in which the mutual separation is much larger than the stellar radii can be approximated as systems of two point masses M_1 and M_2, interacting via gravitational force. Let's call $\mathbf{r}_1$, $\mathbf{r}_2$, $\mathbf{R}_{CM}$ the position of the bodies and of the center of mass, and $\mathbf{r} = \mathbf{r}_2 - \mathbf{r}_1$ the vector connecting the two bodies. The total kinetic energy can be expressed as the sum of the energy associated to the motion of the center of mass and the energy associated to the motion with respect to the center of mass (Landau [17]). The Lagrangian $\mathscr{L}$ then becomes:

$$\mathscr{L} = \frac{1}{2}(M_1 + M_2)|\dot{\mathbf{R}}|^2 + \frac{1}{2}\frac{M_1 M_2}{M_1 + M_2}|\dot{\mathbf{r}}|^2 - V(r) \tag{1}$$

Since the center of mass is either stationary or moving with constant speed, we can neglect its motion and study the system in the center of mass reference frame. In this frame, the problem is reduced to the problem of a single fictitious body of reduced mass $\mu = \frac{M_1 M_2}{M_1 + M_2}$ moving in the external field $V(r)$ with orbital speed:

$$v_{orb} = \dot{r} = \sqrt{\frac{G(M_1 + M_2)}{a}} \tag{2}$$

and energy:

$$E = \frac{1}{2}\mu {v_{orb}}^2 - \frac{G\mu M}{r} \tag{3}$$

The total orbital angular momentum is

$$J = \mu\sqrt{GaM(1 - e^2)} \tag{4}$$

Since it is conserved, therefore the orbit is restricted to a plane and, provided that the energy is negative, it is closed and bound between r_{min} and r_{max}. The ellipse is fully determined by its eccentricity e and by its semi-major axis a (Goldstein [13]):

$$e = \sqrt{1 + \frac{2EJ^2}{\mu^3 G^2 M^2}} \tag{5}$$

$$a = (r_{min} + r_{max})/2 \tag{6}$$

We can express the minimum and maximum distance of the two stars in terms of the semi-major axis and of the eccentricity:

$$r_{min} = a(1-e) \quad r_{max} = a(1+e) \tag{7}$$

The orbit becomes circular when the energy is minimum.
The third Kepler's law gives the binary separation a in terms of the binary period P, which is the fundamental observable quantity.

$$P = 2\pi\sqrt{\frac{a^3}{GM}} \tag{8}$$

After solving the equation of motions for the fictitious body, we return to the original bodies through: $v_{orb,1} = (M_2/M)v_{orb}$ and $v_{orb,2} = (M_1/M)v_{orb}$, where $v_{orb,1}$ and $v_{orb,2}$ are the orbital speeds of the two stars.

2.2 X-ray binary systems

X-ray binaries harbor either a neutron star or a black hole that has a non-compact companion close enough to transfer mass. They are detected through their X-ray emission, while their optical counterpart is very faint compared to X-ray luminosity.

Accretion onto a compact object is the most powerful source of energy we know. Consider a compact object of mass M and radius R_{comp} accreting material at a rate $\dot{M}$, then the accretion rate can be estimated as the gravitational energy which is released at the surface of the compact object per unit of time.

$$L_{\rm acc} = \frac{G\dot{M}M}{R_{comp}} \tag{9}$$

For an accreting object of one-solar mass, $\dot{M}$ needs only to be about $10^{-8}M_\odot$ per year to release a luminosity of $10^{38}erg/s$, which is the order of magnitude of the X-ray galactic sources luminosity.
Using the Einstein mass-energy relation, it becomes clear how the efficiency of the process strongly depends on the compactness of the star:

$$L_{\rm acc} = \xi\dot{M}_{comp}c^2, \quad \xi = \frac{1}{2}\frac{R_s}{R_{comp}} \tag{10}$$

(where R_s is the Schwarzschild radius of the star $2GM_{comp}/c^2$). As a consequence (since withe dwarf radius is 1000 times bigger than a neutron star/black hole radius) the efficiency is larger for neutron stars and black holes than for white dwarfs ($\xi_{NS} \sim 0.1$, $\xi_{BH} \sim 0.06 - 0.42$, $\xi_{WD} \sim 0.001$).
We showed that the luminosity of an accreting source is proportional to the accretion rate, but this does not mean that the accretion power can increase arbitrarily, since radiation itself provides a pressure, the so-called *radiation pressure*.
Let's assume that matter is fully ionized and that it is composed only of Hydrogen. Plasma electrons and photons are subjected to the gravitational force from the compact object, which is much bigger for protons (the mass of the proton is 1836 larger than the mass of the electron):

$$\mathcal{F}_{grav} = \frac{GM(m_p + m_e)}{r^2} \approx \frac{GMm_p}{r^2} \tag{11}$$

For an emitting source of luminosity L, the number of out-flowing photons per unit of surface and unit of frequency is equal to:

$$F_\nu = \frac{L}{4\pi r^2 h\nu} \tag{12}$$

assuming that the photons are emitted isotropically. Upon interaction with an electron, a photon transfers its momentum $p = h\nu/c$ to the electron via *Thomson effect*. The effective area presented by a proton or an electron to a photon is the Thomson cross section σ_T, which, for a particle of charge e and mass m, is:

$$\sigma_T = \frac{2}{3}\left(\frac{e^2}{mc^2}\right)^2 \tag{13}$$

Therefore, the outward radiation pressure on the in-falling matter is mainly exerted by the photons scattering off the electrons. The overall outward force exerted by radiation is:

$$\mathcal{F}_{rad} = \sigma_T F_\nu p = \frac{\sigma_T L}{4\pi r^2 c} \tag{14}$$

Electrostatic attraction keeps electrons and protons coupled so that a proton-electron pair experiences both forces. Now, equating F_{grav} and F_{rad} yields a limiting luminosity of:

$$L_{edd} = \frac{4\pi G M m_p c}{\sigma_T} \sim 3 \times 10^4 \left(\frac{M}{M_\odot}\right) L_\odot \sim 1.3 \times 10^{38} \left(\frac{M}{M_\odot}\right) ergs^{-1} \tag{15}$$

which is called *Eddington Luminosity*.
Typical accretion rates are 4×10^{-10} $M_\odot$/yr for accretion onto a black hole and 1×10^{-9} $M_\odot$/yr onto a neutron star (Tauris & van den Heuvel, 2003).

In a binary where tidal forces have circularized the orbit and brought the two stellar components into syncronized co-rotation, one can define fixed equipotential surfaces in a comoving frame with angular frequency ω, in which both stars lie on the x-axis and the common center of mass is at the origin. A test particle in such a non-inertial frame feels a force $\nabla\Phi_{Roche}$, where Φ_{Roche} is the Roche potential ([28]):

$$\Phi_{Roche}(\mathrm{r}) = -\frac{GM_1}{|\mathbf{r}-\mathbf{r}_1|} - \frac{GM_2}{|\mathbf{r}-\mathbf{r}_2|} - \frac{1}{2}(\boldsymbol{\omega}\times\mathbf{r})^2 \tag{16}$$

where r is the position of the test particle. The last term takes into account the fact that the reference frame is not inertial.
The equipotential surfaces are called *Roche surfaces* and the surface that passes through the inner Lagrangian point L_1 is the so-called *Roche lobe* (see figure 1). At the Lagrangian point, the forces on a test particle from both stars cancel out. Mass that happens to be close to L_1 will then be transferred to the other star.
The geometry of the Roche potential for a binary system with a mass ratio of $q = M_2/M_1$, where M_2 is the donor and M_1 is the neutron star or black hole is shown in figure 1

Since the lobes are not spherical we need some average radius to characterize them; a suitable measure is the radiusR_L of a sphere having the same volume as the lobe. It is a function of the orbital separation a and of the mass ratio q, and it can be approximated as (Eggleton, 1983 [9]):

$$R_L = f(q)a = \frac{0.49q^{2/3}}{0.6q^{2/3} + \ln(1+q^{1/3})}a \tag{17}$$

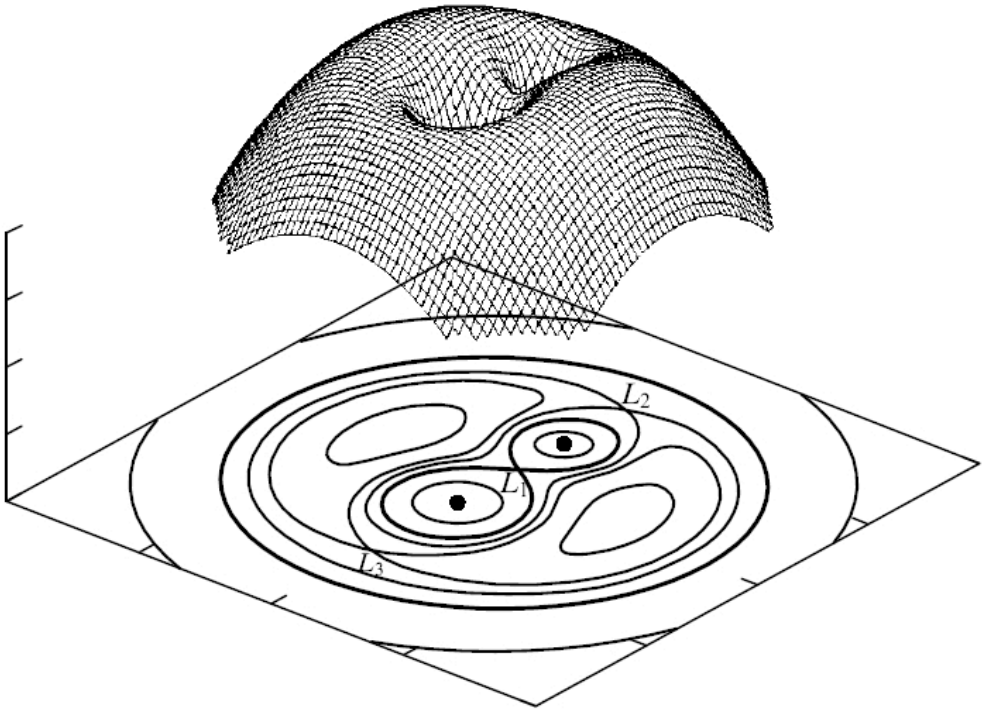

Figure 1: Roche potential. (Tauris & van den Heuvel, 2003 [30])

Setting $q = M_2/M_1$ we get the donor's Roche radius, while taking the inverse of it we obtain the accretor's Roche radius. Material that passes L_1 has a specific angular momentum with respect to the accreting compact object of $L \sim bv_\perp = b^2\omega$, where b is the distance of the accretor from L_1 and $v_\perp$ is the velocity perpendicular to the line joining the two stars. Since angular momentum of the overflowing matter has to be conserved, it cannot be directly accreted onto the compact star, instead it piles up forming an accretion disk. If we assume that the material moves on nearly Keplerian orbits, the differential velocity of the disk is $v_\phi = r\omega = r\sqrt{\frac{GM}{r^3}} \propto r^{-\frac{1}{2}}$.
Adjacent orbits couple to each other via viscous processes, hence, the faster inner orbits lose angular momentum to the slower outer orbits. It's the loss of angular momentum that allows matter to be accreted and it's the friction in the disk that leads to energy radiation. More precisely, according to the *Virial Theorem*, half of the liberated potential energy is converted to kinetic energy. The other half is converted to internal energy, i.e. heat. If a mass m moves in from a radius $r + \Delta r$ to r, an energy

$$\Delta E \approx \frac{GMm}{r^2}\Delta r \tag{18}$$

is released. A ring of thickness Δr will then produce a luminosity of

$$\Delta L \approx \frac{GM\dot{M}}{2r^2}\Delta r \tag{19}$$

If the accretion disk is optically thick, both sides of the disk radiates as a black body:

$$\Delta L = 2 \times 2\pi r \Delta r \sigma_{SB} T(r)^4 \tag{20}$$

By combining equations (19) and (20), we get the radial profile of the temperature:

$$T(r) \approx \left(\frac{GM\dot{M}}{8\pi\sigma_{SB}r^3} \right)^{\frac{1}{4}} \tag{21}$$

A more careful derivation, with a proper modeling of the friction, brings an additional correction factor:

$$T(r) = \left(\frac{3GM\dot{M}}{8\pi\sigma_{SB}r^3} \right)^{\frac{1}{4}} \tag{22}$$

Locally, the spectrum of the disk, i.e. the energy emitted per unit of surface and of frequency, is the Planck spectrum $F_{\nu,BB}$. The overall monochromatic luminosity L_ν is obtained integrating the Planck distribution over the whole disk:

$$L_\nu = 2\int_{r_{min}}^{r_{max}} F_{\nu,BB} 2\pi r dr \tag{23}$$

It turns out that for a given r/R_S, the temperature decreases with the mass of the compact object, because $R_S \propto M_{comp}$; this explains why, for a neutron star or a stellar black hole, the spectrum has a peak in the X-ray band.

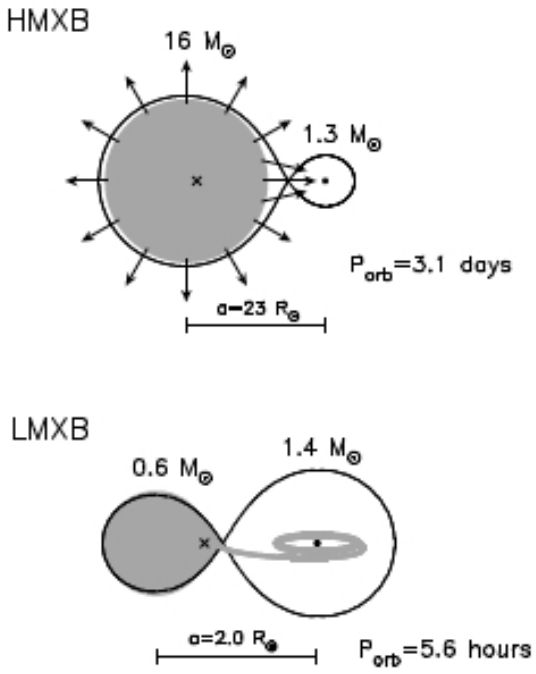

Figure 2: Example of a typical HMXB and LMXB. Tauris & van den Heuvel, 2003 [30])

X-ray binaries are divided into two main class, as according to the mass of the non-compact star: low-mass X-ray binaries (LMXBs) and high mass X-ray binaries (HMXBs) ([29]). In both cases, the accreting star can be either a neutron star or a black hole.

★ HMXB: the donor is a young and massive O/B star with strong winds that sustain the accretion. The orbital periods range from a few hours to several hundreds days. The spectra have characteristic temperatures $k_BT \gtrsim 15keV$ As the donor has only a very limited lifetime, they still reside close to their birth place: therefore, HMXBs are found near star-forming regions in the Galactic disk.

★ LMXB: the donor is a slowly evolving low-mass ($M \leq 1.4M_\odot$) star: it does not have strong winds, hence, it cannot power the X-ray source by the same mechanism as the previous sources. The accretion is driven instead by the Roche Lobe Overflow (RLO), caused by the donor overflowing its Roche lobe, either if the binary separation shrinks (as aresult of orbital angular momentum losses), or the the donor increases its radius. The orbital period range from a few minutes up to several days. The typical photon energy in LMXBs are $k_BT \lesssim 10keV$, and they are usually lower than in the HMXB case.

See figure 2 for a a view of the two types of X-ray binaries.
In the next table we indicate some of the features that help to discriminate between a low-mass and a high-mass X-ray binary ([28]).

Property	LMXB	HMXB
Accreting Object	Low B-field NS or BH	High B-field NS or BH
Companion	Low-mass star, $L_{opt}/L_X \ll 0.1$	High-mass star, $L_{opt}/L_X > 1$
Stellar population	Old: $> 10^9 yr$	Young: $< 10^7 yr$
Accretion mechanism	Roche lobe overflow	Wind
Angular momentum of accreted material	High	Low
Accretion timescale	$10^7 - 10^9 yr$	$10^5 yr$
X-ray spectra	Soft, $k_BT \lesssim 10keV$	Hard, $k_BT \gtrsim 15keV$

Table 1: Summary of the differences between LMXB and HMXB

2.2.1 Black hole X-ray binary system

There are 23 confirmed black holes X-ray binaries in our Galaxy (Özel et al., 2010). Black holes X-ray binaries provide astronomers with the chance of investigating stellar black holes candidates: as a matter of fact, the so-called *mass function* gives a lower limit on the mass of the unseen companion.
The mass function is a function of the masses of the two stars and of the inclination angle of the system; it's an observable quantity, since it can also be expressed as a combination of the orbital period and the semi-amplitude of the orbital velocity. These two parameters are determined dynamically studying the radial velocity curve of the optical counterpart. The mass function is derived below.

If spectral lines of the companion star can be measured, we have a *single-line spectroscopic binary*. In this case it is possible to measure the orbital velocity of the companion star, projected onto the line of sight, $v_{2,los}$, via the Doppler effect. If M_2 is the mass of the companion star, M_1 the mass of the black hole and M the total mass, we can express the semi-amplitude of the radial curve, K, as:

$$K = v_{2,orb} \sin i = \frac{M_1}{M} v_{orb} \sin i \tag{24}$$

If the velocity along the line of sight is plotted against time, we can directly infer the orbital period P and the semi-amplitude of the velocity K. Taking a special combination of these two parameters, we get the mass function:

$$f(M) \equiv \frac{PK^3}{2\pi G} \tag{25}$$

Once we measure the mass function, we get a handle of the *unseen* object. As a matter of fact, it can also be expressed in terms of the mass ratio:

$$f(M) = \frac{M_2 sin^3 i}{(1+q)^2} \tag{26}$$

As $(\sin i^3) \leq 1$ and $(1+q)^{-2} < 1$, the mass function of the observed star gives a lower limit for the mass of the black hole: $M_1 > f(M)$.
The identification of a compact object as a black hole requires not only an accurate observational estimate of its mass, but also knowledge of the maximum mass of a neutron star for stability against collapse into a black hole. The maximum mass of a neutron star depends on the equation of state for dense matter. Rhoades & Ruffini ([27]), assuming the *Tolman-Oppenheimer-Volkoff* equations as the equations of state for a neutron star, derives a maximum limit for the mass of a neutron star: $M_{ns} \leq 3.2\ M_\odot$.

Özel et al. (2010) used the dynamical mass measurements of black holes in low-mass X-ray binaries to infer the stellar black hole mass distribution in the Galaxy. They found that the observations are best described by a narrow mass distribution centered at $7.8 \pm 1.2\ M_\odot$. More precisely, the cut-off of the distribution at the low end is $\gtrsim 5\ M_\odot$, indicating a significant lack of black holes in the $\sim 2-5\ M_\odot$ range; at the high-mass end the distribution declines rapidly for $M \gtrsim 14\ M_\odot$.

Of the 23 BH candidates, 17 are found in LMXBs. In table 2 we present the mentioned

population (Özel et al., 2010 [24]). For each of them, we indicate their X-ray intensity, their latitude b,longitude l and orbital period P, and the current constraint on their distance.
For most of the BH-LMXBs it is not feasible to obtain a trigonometric parallax measurement. Instead the distance is generally determined by comparing the derived absolute magnitude of the optical counterpart with the apparent magnitude (Nelemans & Jonker, 2004 [15]). A first guess of the distance can be obtained by assuming that the absolute magnitude is that of a main-sequence star of the observed spectral type. Specifying the distance to the object and its longitude l and latitude b, its position is univocally determined. We would like to remind that the galactic longitude is measured in the plane of the Galaxy using an axis pointing from the Sun to the galactic center, while the galactic latitude is measured from the plane of the galaxy to the object using the Sun as vertex ([4]).

	Common name or prefix	Coordinate Name	Max. Int. (Crab)	l (deg)	b (deg)	P (hr)	d (kpc)
1	GS	1354-64	0.12	310.0	-2.8	61.1	>25
2	4U	1543-47	15	330.9	+5.4	26.8	7.5 ± 0.5
3	XTEJ	1550-564	7.0	325.9	-1.8	37.0	4.4 ± 0.5
4	GROJ	1655-40	3.9	345.0	+2.5	62.9	3.2 ± 0.5
5	GX339-4	1659-487	1.1	338.9	-4.3	42.1	9 ± 3
6	V4641 Sgr	1819.3-2525	13	6.8	-4.8	67.7	9.9 ± 2.4
7	GRS	1915+105	3.7	45.4	-0.2	739	9 ± 3
8	GS	2023+338	20	73.1	-2.1	155.3	2.39 ± 0.14
9	GROJ	0422+32	3	166.0	-12.0	5.1	2 ± 1
10	A	0620-003	50	210.0	-6.5	7.8	1.06 ± 0.12
11	GRS	1009-45	0.8	275.9	+9.4	6.8	3.82 ± 0.27
12	XTEJ	1118+480	0.04	157.6	+62.3	4.1	1.7 ± 0.1
13	Nova Mus 91	1124-683	3	295.3	-7.1	10.4	5.89 ± 0.26
14	XTEJ	1650-500	0.6	336.7	-3.4	7.7	2.6 ± 0.7
15	Nova Oph 77	1705-250	3.6	358.2	+9.1	12.5	8.6 ± 2.1
16	XTEJ	1859+226	1.5	54.1	+8.6	9.2	8 ± 3
17	GS	2000+251	11	63.4	-3.0	8.3	2.7 ± 0.7

Table 2: Properties of 17 BH-LMXBs. (Özel et al. 2010 [24]).

3 Binary Stellar Evolution from ZAMS to SN: the LMXB case

A LMXB is only a snapshot in the life of a binary system. So how did such systems form and how do they evolve?
Low mass X-ray binary systems are initially formed by two main sequence stars with an extreme mass ratio. One star is much more massive than the other, it will then evolve much more rapidly: this means that it will leave the main-sequence on a shorter time scale. The full evolutionary history of a LMXB can be summarized as follow:

- ★ Due to the evolution of the progenitor of the BH, a first stage of mass transfer begins. At this stage, the mass transfer is violent and leads to the formation of a common envelope.
- ★ The Helium star explodes as a supernova. The explosive mass loss, and possibly a natal kick imparted to the compact object at the time of the core collapse, affects the orbital properties of the binary.
- ★ Once the compact object is formed, the binary will then evolve in the Galactic potential up to the present day for the main sequence time of the companion star. In the meantime, binary properties are subjected to changes, due to the tidal evolution.
- ★ Today, after the binary is visible through its X-ray radiation: a second stage of mass-transfer is now at work.

In figure 3 we show a representation for a binary system that leads to a NS-LMXB: from ZAMS to the observed X-ray emission. Throughout the next discussion, by M_1 we mean the mass of the progenitor of the black hole, and by M_2 we mean the star that is currently transferring mass.

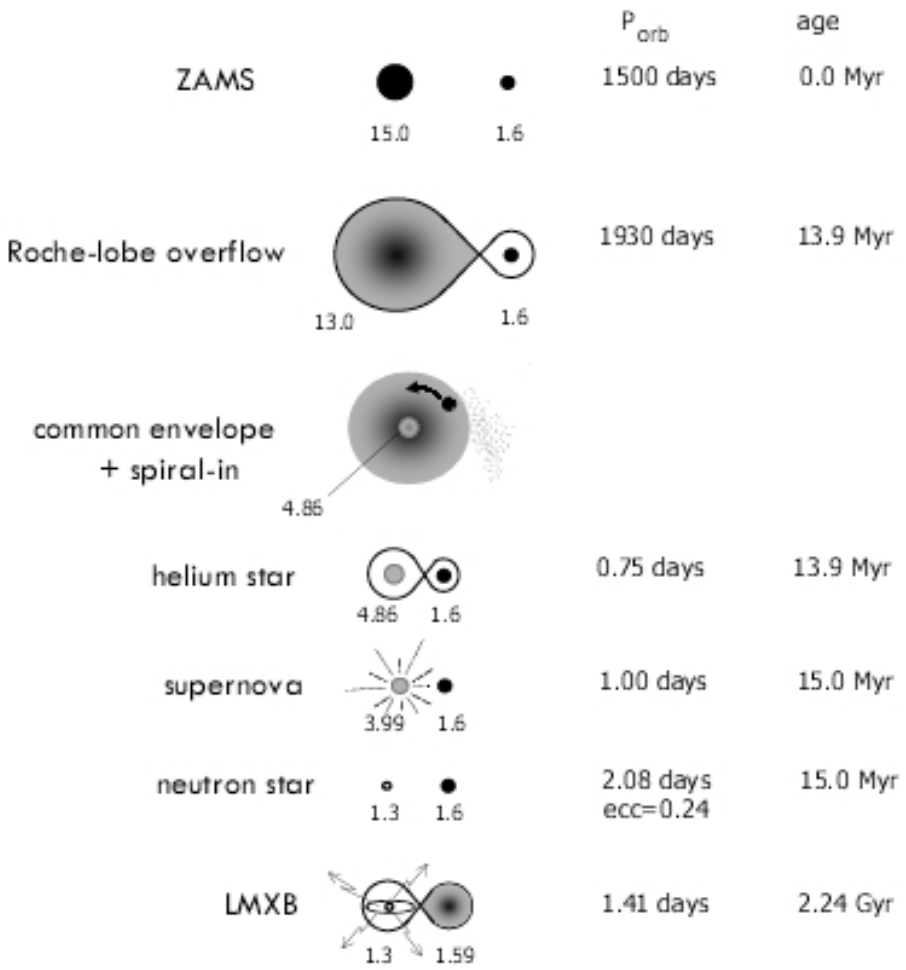

Figure 3: Evolution of a binary system eventually leading to a NS-LMXB. Tauris & van den Heuvel, 2003 [30]

3.1 What happens before the Supernova explosion

Before investigating how stellar evolution affects the orbital properties of a binary system, we would like to overview three fundamental timescales that characterize single star evolution (Tauris & van den Heuvel, 2003 [30]). When the thermal equilibrium of a star happens to be disturbed, the star will restore it on the so-called *thermal timescale*, which is the time it takes to emit all of its thermal energy content at the present luminosity L:

$$\tau_{th} = \frac{GM^2}{RL} \simeq 30(M/M_\odot)^{-2} \text{ Myr} \tag{27}$$

where the current luminosity L can be approximated as $L \approx \left(\frac{M}{M_\odot}\right)^{3.5} L_\odot$ (which is the *mass-luminosity* relation for a main-sequence star. When is the hydrostatic equilibrium of a star to be disturbed (e.g. because of mass loss), the star will restore this equilibrium on a *dynamical timescale*:

$$\tau_{dyn} = \sqrt{\frac{R^3}{GM}} \simeq 30(R/R_\odot)^{3/2}(M/M_\odot)^{-1/2} \text{ min} \tag{28}$$

The *nuclear timescale*, instead, which is the time needed for the star to exhaust its nuclear fuel reserve:

$$\tau_{nuc} \simeq 10(M_\odot/M)^{2.5} \text{ Gyr} \tag{29}$$

This is, in other words, the main-sequence time of the star.

Initially, on the ZAMS, the binary consists of two stars in wide circular orbits and with a large mass ratio. When the progenitor of the compact object, which evolves much faster then the other, runs out of Hydrogen in its core, it evolves off the main sequence reaching the red giant branch, while the companion star, which is far less massive, is still on the main sequence. Thanks to the expansion of its outer layers, the red-giant star overflows its Roche lobe and mass transfer sets in.
We will always refer to the donor star as M_2 and to the accreting star as M_1. The time scale of the MT depends on how the Roche radius dependence from time compared with the star radius time dependence:

$$\dot{R}_1 = \left.\frac{\partial R_1}{\partial t}\right|_{M_1} + R_1\alpha_2\frac{\dot{M}_1}{M_1} \tag{30a}$$

$$\dot{R}_L = \left.\frac{\partial R_L}{\partial t}\right|_{M_1} + R_L\alpha_L\frac{\dot{M}_1}{M_1} \tag{30b}$$

The second term on the right-hand sides takes into account the change in R_1 and R_L due to the mass transfer. These relations are usually fit by a power-law, $R_{1,L} \sim M_1^{\alpha_l,\alpha_1}$, where the power-law indexes are:

$$\alpha_1 \equiv \frac{\partial \log R_1}{\partial \log M_1} \qquad \text{cf.} \qquad \alpha_L \equiv \frac{\partial \log R_L}{\partial \log M_1} \tag{31}$$

The first term in the first equation is due to the expansion of the donor star as a result of nuclear burning (e.g. shell Hydrogen burning on the RGB) and the first term in the second equation represents changes in R_L which are not caused by mass transfer-such as orbital decay due to gravitational wave radiation. We will now consider what happens to the orbital separation (and, consequently, to the Roche radius).
Mass transfer tends to change the orbital separation too, because of redistribution of angular momentum between the two stars: logarithmically differentiating eq. (4) with respect to time, we obtain the equation for the time evolution of the binary separation ([11]):

$$\frac{\dot{a}}{a} = 2\frac{\dot{J}}{J} - 2\frac{\dot{M}_1}{M_1} - 2\frac{\dot{M}_2}{M_2} + \frac{\dot{M}_1 + \dot{M}_2}{M} \tag{32}$$

At this stage mass transfer happens to be from the more massive star to the less massive one: it shrinks the Roche lobe down (and any angular momentum loss accentuates the shrinking). As a matter of fact, if momentum is conserved and the more massive star is becoming less and less massive, the companion star has to move further in in order to keep the center of mass fixed. The shrinking of the orbital separation causes a shrinking of the Roche radius, while the radius of the star keeps expanding. The overflow becomes then very violent, proceeding on a *dynamical* or *thermal* timescale, depending on whether the star's envelope is convective or radiative. Since matter is transferred to the accretor more rapidly than the latter one can accept it, it cannot be accreted, instead, it forms an envelope which engulfs both stars (the so-called *common envelope*). The envelope exterts a drag force on the orbiting stars and thereby extracts energy at the expense of the orbital energy. The energy extracted from the orbit is deposited in the envelope as thermal energy and can help the system to get rid of the envelope.
A simple estimation of the reduction of the orbital separation can be found assuming that a fraction η of the gravitational binding energy released by the spiraling together of the non-evolved star and the giant core is used to overcome the gravitational bond between envelope and core.
The binding energy of the envelope to the giant core can be expressed as (Davies et al., 2001 [7]):

$$E_{env} = \frac{G(M_{He} + M_e)M_e}{\lambda R_{L,1}(q, a_i)} \tag{33}$$

where λ is a parameter which depends on the stellar mass-density distribution ($\lambda \sim 0.5$ from detailed stellar models).
The change in binding energy of the secondary is given by:

$$\Delta E_g = \frac{GM_2M_c}{2a_{\text{post-ce}}} - \frac{GM_2(M_e + M_c)}{2a_{\text{pre-ce}}} \tag{34}$$

where M_2 is the main sequence star, M_e is the mass of red-giant envelope, M_{He} is the mass of the Helium core, $R_{L,1}$ is the Roche-lobe of the evolved star. Then $M_{1,i} = M_e + M_c$. Thus, we can find the orbital separation by solving:

$$E_{env} = \eta \Delta E_g \tag{35}$$

We get:

$$a_{\text{post-ce}} = a_{\text{pre-ce}} \left[\frac{2(M_{1,i} M_e) a_{\text{pre-ce}}}{\eta \lambda M_{He} M_2 R_{L,1}(q, a_{\text{pre-ce}})} + \frac{M_{1,i}}{M_{He}} \right]^{-1} \tag{36}$$

What is left after the common envelope phase, is a naked Helium star of mass M_{He} and a companion star of mass almost unchanged M_2, provided that η is sufficiently large and that main-sequence star doesn't fill its Roche lobe at the end of the CE (otherwise the two stars will merge):

$$R_2 > R_{L,2}(q_{post-CE}, a_{\text{post-ce}}) \tag{37}$$

Tauris & van den Heuvel [30] fitted the helium star radius as a function of the mass: $R_{He} = 0.212 (M_{He}/M_\odot)^{0.654} R_\odot$, while the radius of the companion, that is still on the main sequence, is $R_2 \sim \left(\frac{M}{M_\odot}\right)^{0.8} R_\odot$. The orbital separation has decreased considerably thanks to the common envelope: it is quite often reduced by a factor ~ 100, causing the final orbital separation
to be $\gtrsim$ few $R_\odot$. Typical orbital velocities associated to this separation are of the order of $\sim$ few 100 km/s.

3.2 Effects of a supernova explosion (What we know from neutron stars)

Since the suggestion of Baade and Zwicky ([2]) and the discovery of pulsars in the Crab and Vela supernova remnant, it is accepted that neutron stars are formed in a *supernova* explosion (SN). This is also believed to be true for black holes.
A brief discussion on how black holes and neutron stars are formed is needed.

A massive star ($M \gtrsim 10\ M_\odot$) evolves through cycles of nuclear burning alternating with stages of exhaustion of nuclear fuel in the stellar core until its core is made of iron, at which point further fusion requires, rather than releases, energy. The core mass of such a star become larger than the *Chandrasekhar limit*, the maximum mass possible for an electron-degenerate configuration ($\sim 1.4\ M_\odot$). Therefore the core implodes to form a neutron star or black hole. The gravitational energy released in this explosion ($4 \times 10^{53} erg$) is far more than the binding energy of the stellar envelope, causing the collapsing star to violently explode and eject the outer layers of the star, in the supernova event. The final stages during and beyond carbon burning are very short lasting ($\sim$ 60yr for a 25 $M_\odot$ star), because most of the nuclear energy generated in the interior is liberated in the form

of neutrinos which freely escape without interaction with the stellar gas and thereby lowering the outward pressure and accelerating the contraction and nuclear burning.
To make a black hole, the initial ZAMS stellar mass must exceed at least 20 $M_\odot$, or possibly, 25 $M_\odot$ and the mass of the Helium core greater than 8 $M_\odot$ (Tauris & van den Heuvel, 2003 [30]): *neutron degeneracy pressure* cannot manage to sustain the core against gravitational collapse. It should be stressed that the actual values that discriminate between one compact object and another are only known approximately due to the considerable uncertainty in our knowledge of the evolution of massive star.

What happens when the supernova occurs in a binary system?
After the binary red-giant star has lost its H-envelope (and possibly also its He-envelope) during the CE evolution, it will collapse and explode as a supernova. All observed neutron stars in binary pulsars seem to have been born with a canonical mass of $1.3 - 1.4 M_\odot$. Neutron stars in LMXBs might afterwards possibly accrete up to $\sim 1 M_\odot$ before collapsing further as a black hole.
The supernova will of course be asymmetric in the center of mass frame of reference: the system will then suffer a recoil due to the instantaneous mass loss. Precisely, the center of mass of the ejected matter will continue to move with the orbital velocity of the black hole progenitor. To conserve momentum, the binary has to move in the opposite direction. We will call the velocity of the new center of mass with respect to the old one as *system velocity*, while with *mass loss kick* (MLK) we will be referring to its modulus.
Asymmetries in the explosion can instead impose large velocities to the remaining black hole itself: we will refer to these velocities as *natal kicks*. What happens is that, if the mass is ejected non-isotropically, the remaining compact star suffers a recoil; asymmetries don't need to be high: it is possible to show that even a small asymmetry of 1% can lead to very large natal kicks of few hundreds km/s. We then have three velocities interplaying: mass-loss kick, natal kick and system velocity: systems surviving the SN will receive a recoil velocity v_{sys} from the combined effect of instant mass loss and a kick.

In the next two sections we will investigate the effects of mass loss on the orbital properties of the binary, starting from some assumptions: the initial orbit is circular, we neglect the change in the companion star's velocity due to the impact of the ejected shell, we assume that the explosion is instantaneous (which means that gravitational decoupling time scale of the ejecta star is short in comparison with the orbital timescale). Our calculations will be held in a reference frame centered at the center of mass, with both of the two stars lying on the y-axis.

3.2.1 Symmetric supernova explosion: Mass-loss kick (MLK)

Consider a binary with orbital separation a, companion star M_2 and progenitor of the compact object of mass M_1. After the explosion, the compact object has mass $\widetilde{M_1}$, we will call the mass loss $\Delta M = M_1 - \widetilde{M_1}$. Generally, primed quantities will refer to post-SN quantities. In first approximation, we assume that the relative velocity between the non-exploding star and the remnant is still close to its original value: $v_{orb} = \sqrt{GM/a_{\text{pre-sn}}}$. We can then compute the energy of the system immediately after the explosion:

$$E' = \frac{1}{2}\mu' {v_{orb}}^2 - \frac{G\mu' M'}{a_{\text{pre-sn}}} = \frac{G\mu'}{2a_{\text{pre-sn}}}\left(\frac{M}{2} - M'\right) \tag{38}$$

where M is the initial total mass, M' is the final total mass and a is the separation between the stars at the moment of the explosion.
In order for the energy to be negative, we must have:

$$\Delta M < \frac{M}{2} \tag{39}$$

This means that the binary only survives if less than half of its total mass is ejected. Generally, a high companion mass makes the survival of the binary more probable. We will see how natal kicks might weaken this strong constraint.
We can compute the velocity of the new center of mass with respect to the old one (that is, the mass-loss-kick):

$$v_{sys} = \frac{\widetilde{M_1} v'_{orb,1} + M_2 v_{orb,2}}{\widetilde{M_1} + M_2} \tag{40}$$

After expressing the orbital velocity in terms of the semi-major axis, we get:

$$v_{sys} = \frac{\Delta M}{M'}\frac{M_2}{M}\sqrt{\frac{GM}{a_{\text{pre-sn}}}} \tag{41}$$

The mass loss changes of course the orbital parameters. As a matter of fact, as matter is lost from the system, the bounding energy of the system decreases: this means that the the orbit becomes eccentric. The new orbital parameters are entirely determined by the amount of mass lost from the system during the explosion.
In particular, we can estimate the post-SN semi-major axis via conservation of energy. Since the post-SN energy (cf. (19)) can also be expressed as $-G\mu' M'/2a'$, we then have an expression for the post-SN semi-major axis in terms of the initial semi-major axis:

$$a_{\text{post-sn}} = \frac{a_{\text{pre-sn}}}{2 - \frac{M}{M'}} \tag{42}$$

It is straightforward to estimate the binary eccentricity, if we assume, reasonably, that the distance a_i between the two stars before the supernova is the periastron distance after the explosion (Bhattacharya & van den Heuvel, 1991 [3]):

$$e = \frac{\Delta M}{M'} \tag{43}$$

Due to tidal interaction between the two stars, the orbital separation tends to circularize. In the simplistic hypothesis that angular momentum is conserved in the process, we get an expression for the circularized semi-major axis in terms of the post-SN one:

$$a_{circ} = (1 - e)(1 + e)a_{\text{post-sn}} \tag{44}$$

For $e \sim 1$, we get:

$$a_{circ} \sim 2a_{\text{post-sn}}(1 - e) \tag{45}$$

At a first glance, one could infer the pre-SN binary separation from the observed circularized one, as if the binary experienced just two phases, the SN explosion and the circularization after it. Yet, this is too naive: the binary, during its secular evolution in the Galactic potential, might experience the shrinking of its orbit due to different mechanism (such as tidal interaction or gravitational wave emission). We have to take into account these effects if we want to have a sensible estimate on the initial parameters of the binary.

It is interesting to highlight that a high-mass X-ray binary system will suffer from a smaller recoil compared to a low-mass one, because of the higher mass of the companion star. We then expect HMXBs to be much closer to the Galactic plane, while LMXBs to be more spread around the Galactic plane. Also, we should not forget that HMXBs are younger than LMXBs: they did not have the time yet to move significantly out of the Galactic plane.

3.2.2 Asymmetric supernova explosion: Natal Kick (NK)

It is almost universally accepted that neutron stars receive a substantial kick when they are born: this scenario fits well the high space velocities (typically ~ 400 kms^{-1}) inferred from the observed distribution of pulsars (Lyne & Lorimer, 2004 [18]). However, neither the exact distribution of kick velocities nor the physical origin of these kicks are properly understood.
It is still an open question whether black holes receive kicks as well. We will now investigate in detail what it is known to happen when a star collapses into a neutron star.
If the supernova ejects mass non isotropically, the remnant will suffer from a recoil, whose magnitude follows directly from conservation of momentum. The natal kick adds vectorially to the orbital velocity of the compact star with no preferred direction with respect to the orbital plane: this hypothesis is very much acceptable, since the escaping neutrinos from deep inside the collapsing core are not aware that they are members of a binary system. Geometrically, the direction is univocally defined via θ, which is the angle between the natal kick and the orbital plane, and ϕ, which is the direction between the direction of natal kick projection on the orbital plane and the direction of the initial orbital speed. In the next figure the geometry of the vectors is clear: The new orbital speed of the remnant will then be:

$$\mathbf{v}_1' = \mathbf{v}_1 + \mathbf{v}_{nk} \tag{46}$$

This effect will then combine with the effect of the mass loss kick to give the space velocity of the system with respect to the old center of mass.
Because of the received kick, the orbit of the compact star will become eccentric and, generally speaking, the closer in magnitude is the kick to the orbital velocity, the more it will affect the binary properties. Crucial is the direction of the kick: when the kick happens to be in the good direction, they can help the system to stay bound, even if more than half of the mass is lost from the system.
We will call M the total initial mass, M' the total post-SN mass, $\widetilde{M_1}$ the mass of the compact star and M_2 the mass of the companion star and μ' the post-SN reduced mass.

The post-SN energy of the system is:

$$E' = \frac{1}{2}\mu' |\mathbf{v}_{orb} + \mathbf{v}_{nk}|^2 - \frac{G\mu' M'}{a_{\text{pre-sn}}} \tag{47}$$

Expressing the orbital velocity in terms of a, we get:

$$E' = -\frac{G\widetilde{M_1} M_2}{2a_{\text{pre-sn}}} \left\{ 2 - \frac{M}{M'} \left[1 + 2\frac{v_{nk}}{v_{orb}} \cos\phi \cos\theta + \left(\frac{v_{nk}}{v_{orb}} \right)^2 \right] \right\} \tag{48}$$

For the energy to be negative, we need the whole expression between curly brackets to be positive: we obtain a condition on the direction of the kick.

$$\cos\phi \cos\theta < \frac{1}{2} \frac{v_{orb}}{v_{nk}} \left[\frac{2M'}{M} - 1 - \left(\frac{v_{nk}}{v_{orb}} \right)^2 \right] \tag{49}$$

Then, since $\cos\phi\cos\theta$ cannot be less than -1, we have also to require that:

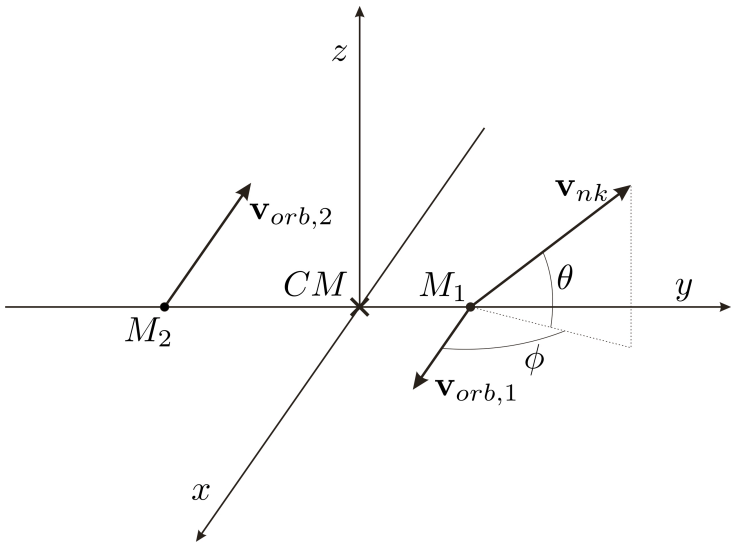

Figure 4: Sketch showing the binary system and supernova kick geometry.

$$v_{nk} < \left(1 + \sqrt{\frac{2M'}{M}}\right) v_{orb} \tag{50}$$

in case the mass loss is more than half of the total initial mass, the last condition has to be valid together with:

$$v_{nk} > \left(1 - \sqrt{\frac{2M'}{M}}\right) v_{orb} \tag{51}$$

Here we evidently see how the system might remain bound thanks to the kick. Let's calculate now the dynamical changes of a binary surviving the explosion.
We can express the system velocity, v_{sys}, i.e the velocity that the binary received as a result of the explosion. It just the velocity of the post-SN CM relative to the initial CM frame. It is not a unique function of the natal kick velocity, of the mass loss and of the

initial orbital velocity, since it depends also on the direction of the kick. In terms of the initial masses, the mass loss and the angles θ and ϕ, as follows.
Here are the x,y,x-components of the space velocity:

$$v_{sys,x} = \frac{\widetilde{M_1}\left(v_{orb,1} + v_{nk}\cos\theta\cos\phi\right) - M_2 v_{orb,2}}{\widetilde{M_1} + M_2} \tag{52a}$$

$$v_{sys,y} = \frac{\widetilde{M_1}\left(v_{orb,1} + v_{nk}\cos\theta\cos\phi\right)}{\widetilde{M_1} + M_2} \tag{52b}$$

$$v_{sys,z} = \frac{\widetilde{M_1} v_{nk}\sin\theta}{\widetilde{M_1} + M_2} \tag{52c}$$

Combining this three components, we get:

$$v_{sys} = \frac{v_{orb}}{\widetilde{M_1} + M_2} \times \left[\left(\frac{\mu\Delta M}{M_1}\right)^2 - 2\frac{\mu\Delta M\widetilde{M_1}}{M_1}\frac{v_{nk}}{v_{orb}}\cos\phi\cos\theta + \left(\widetilde{M_1}\frac{v_{nk}}{v_{orb}}\right)^2\right]^{1/2} \tag{53}$$

We can compute the new semi-major axis remembering that the $E' = -G\mu' M'/2a_{\text{post-sn}}$ and equating it to the expression in equation (48):

$$a_{\text{post-sn}} = \frac{a_{\text{pre-sn}}}{2 - \frac{M}{M'}\left[1 + 2\frac{v_{nk}}{v_{orb}}\cos\phi\cos\theta + \left(\frac{v_{nk}}{v_{orb}}\right)^2\right]} \tag{54}$$

This equation reduces to equation (42) when $v_{nk} = 0$.
Because of the kick given to the remnant star, the system becomes highly eccentric ($e \sim 1$), since the orbital energy increases. If the eccentricity of the post supernova system is measured, we can have an estimate on the post-SN separation, without having to take into account the angle between the natal kick and the orbital speed. As a matter of fact, it is fair claiming that the pre-SN orbital separation must be larger then the new periastron separation and smaller than the new apastron distance:

$$a_{\text{post-sn}}(1-e) < a_{\text{pre-sn}} < a_{\text{post-sn}}(1+e) \tag{55}$$

Currently, neither the exact distribution of kick velocities nor the physical origin of these kicks are properly understood. Neutron star kicks have been modeled since the early nineties, when Lyne and Lorimer, looking at the sky distribution of radio pulsars and reassessing pulsars distances, derive a mean pulsar birth velocity of $\sim 450 \pm 90$ km/s, with very few low-velocity pulsars. Since then, there have been other attempts to infer the intrinsic natal kick distribution from the observed pulsar velocities. In my work, I am referring to the *natal kick distribution* proposed by Hansen & Phinney ([14]). For the modulus of the kick velocity they proposed a maxwellian probability distribution with velocity dispersion $\sigma_v = 190$ km/s (implying a mean velocity of ~ 300 km/s), again containing very few low-velocity pulsars:

$$f(v_{nk}) = \sqrt{\frac{2}{\pi}}\frac{v_{nk}^2}{\sigma_v^3}e^{-\frac{v_{nk}^2}{2\sigma_v^2}} \tag{56}$$

We plot in the next figure the distribution function.

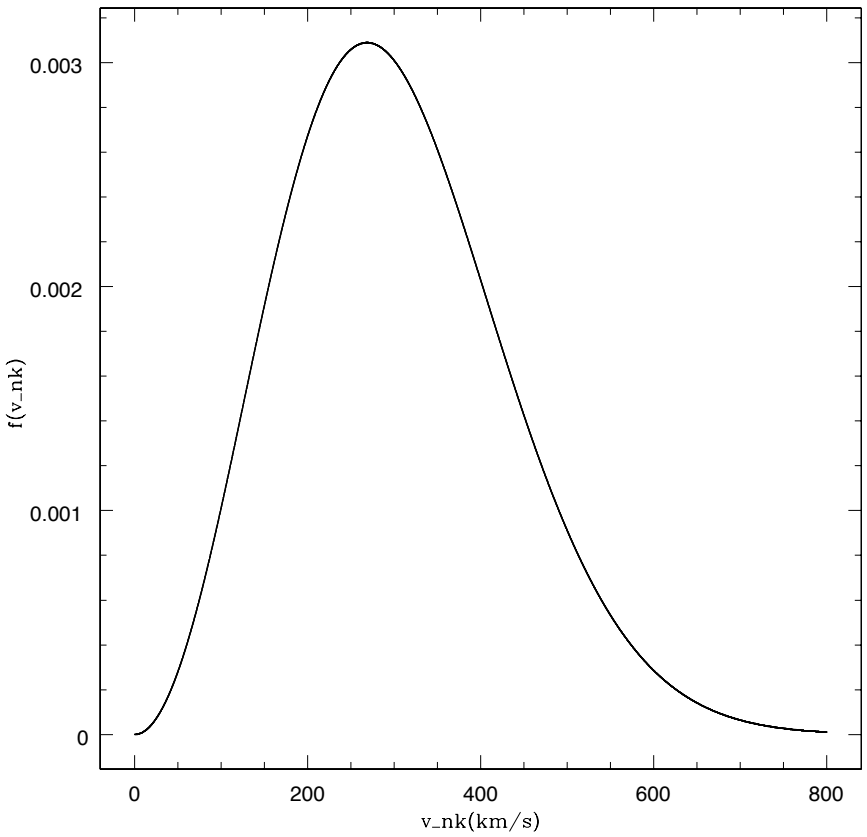

Figure 5: Hansen & Phinney distribution for the natal kick ([14]).

Natal kicks of magnitude $\sim$ few hundreds km/s happen to be of the same order of magnitude of the typical orbital binary speed. For a system consisting of a black hole of mass $\widetilde{M_1} = 6M_\odot$ and of a companion star of mass $M_2 = 1.5$ at a distance of 10 $R_\odot$, we get (using equation eq. (2) and expressing the masses in units of solar mass and the orbital separation in terms of the radius of the sun):

$$v_{orb} = \sqrt{\frac{GM_\odot}{R_\odot}\frac{(\widetilde{M_1} + M_2)}{a}} \sim 436\sqrt{\frac{(\widetilde{M_1} + M_2)}{a}} \sim 300 \text{ km/s} \tag{57}$$

If natal kicks were much lower, let's say around tens km/s, they wouldn't affect significantly the binary properties: this would affect the probability for the system to remain bound after the explosion.
Recently (Podsiadlowsky et al. 2005 [26]) it has been proposed a *dichotomous* scenario for neutron star kicks, in order to solve the retention problem in globular cluster. There is good observational and theoretical evidence that some of the massive globular clusters in our Galaxy contain more than $\sim$ 1000 neutron stars. However, assuming a natal kick of few hundreds km/s, neutron stars would not be retained, since the escape velocity from a Globular cluster is $\lesssim$ 50 km/s. Within this framework, the natal kick distribution is modeled as two maxewellians, one picked at lower velocities, the other picked at higher ones.

4 The potential of our Galaxy

The potential of a galaxy is usually represented as the superposition of several potentials. Once we have the density profile, we obtain the correspondent potential via the *Poisson equation*: $\nabla^2\Phi(\mathbf{r}) = 4\pi G\rho(\mathrm{r})$.
For our Galaxy, we refer to the model presented by Paczynski ([25]): the total mass distribution is made up of three components, the *disk*, the *spheroid* and the *halo*. The overall potential is cylindrically symmetric, hence it is convenient to use a cylindrical coordinate system (R, z, ϕ) with the Galactic center at the origin; R is the distance of the object projected over the Galactic plane, z is the height over the plane and ϕ is the polar angle in the plane (we set $\phi = 0$ for the Sun). The distance d is then $\sqrt{R^2 + z^2}$.
For the disk and the spheroid, Paczynski uses the superposition of two Miyamoto-Nagai potentials:

$$\Phi_{\mathrm{d}}(R,z) = -\frac{GM_{\mathrm{d,s}}}{\sqrt{R^2 + \left(a_{\mathrm{d,s}} + \sqrt{z^2 + b_{\mathrm{d,s}}^2}\right)^2}} \tag{58a}$$

$$\Phi_{\mathrm{s}}(R,z) = -\frac{GM_{\mathrm{s}}}{\sqrt{R^2 + \left(a_{\mathrm{s}} + \sqrt{z^2 + b_{\mathrm{s}}^2}\right)^2}} \tag{58b}$$

This kind of potential is used in the case of symmetry about the z-axis. The parameters a and b have the dimension of a length and determine the size and the flattening of the system. The parameter M is the total mass of the component. Here are the parameters for the Paczynski model:

$$a_d = 3.7kpc, \qquad b_d = 0.20kpc, \qquad M_d = 8.07 \times 10^{10} M_\odot \tag{59a}$$

$$a_s = 0, \qquad b_s = 0.277kpc, \qquad M_s = 8.07 \times 1.12^{10} M_\odot \tag{59b}$$

$$\tag{59c}$$

A double Miyamoto-Nagai potential is not enough to represent the overall Milky Way. Astronomers realized this looking at the *rotation curve* in the Galaxy; we will see how the radial dependence of the circular velocity differs from the rotation curve we would obtain if all the mass was concentrated in the center. One must add a third component: the so-called *halo* component, which is mainly formed by dark matter and whose outer limit is $\sim 41kpc$.
The halo is modeled as a softened *isothermal sphere* (here $r^2 = R^2 + z^2$):

$$\rho_{\mathrm{h}}(r) = \frac{\rho_c}{1 + (r/r_c)^2} \tag{60}$$

This model leads to a potential:

$$\Phi_{\mathrm{h}}(r) = \frac{GM_{\mathrm{c}}}{r_{\mathrm{c}}}\left[\frac{1}{2}\ln\left(1 + \frac{r^2}{r_{\mathrm{c}}^2}\right) + \frac{r_{\mathrm{c}}}{r}\arctan\left(\frac{r}{r_{\mathrm{c}}}\right)\right] \tag{61}$$

The central density is ρ_c, and the two parameters are connected via $M_c = 4\pi\rho_c r_c^3$, where $r_c = 6.0kpc$ and $M_c = 5.0 \times 10^{10} M_\odot$. The overall potential is then given by:

$$\Phi(\mathbf{r}) = \Phi_d(R,z) + \Phi_s(R,z) + \Phi_h(r) \tag{62}$$

The parameters of the model are set so that the Sun is in circular orbit around the Galactic center (see section 4.1.)

4.1 Trajectories in the Galactic potential

Investigating trajectories of stars in the Milky Way means integrating the motion of a particle in the above-mentioned potential. In order to do so, we need to solve a system of coupled three second-order ordinary differential equations (ODE). Since the potential is cylindrically symmetric, we can use the constant z-component of the angular momentum in order to reduce the number of equations: we get to four first-order ODEs.

$$\begin{aligned} \frac{dR}{dt} &= v_R, \qquad \frac{dv_R}{dt} = -\left(\frac{\partial\Phi}{\partial R}\right)_z + \frac{j_z^2}{R^3}, \\ \frac{dz}{dt} &= v_z, \qquad \frac{dv_z}{dt} = -\left(\frac{\partial\Phi}{\partial z}\right)_R \end{aligned} \tag{63}$$

Setting the initial conditions, we can then compute the forward trajectory of the binary by numerical integration (in particular, 4th-order *Runge-Kutta method* will be used). As concerning the units, it is common practice to express distances in kpc, time in 10^6 year (Sun's orbital period is $\sim 3\times10^8$ years), velocities in km/s and mass in solar mass ($1M_\odot = 1.989 \times 10^{30} kg$).
Using the equation for the time evolution of the radial velocity, it is possible to obtain the rotation curve, i.e. the circular velocity as a function of the distance R: $v_\phi = v_\phi(R)$. For a perfectly circular orbit, it is legitimate to put $\frac{dv_R}{dt} = 0$; expressing then the z-component of the angular momentum as $j_z = Rv_\phi$ and calculating the R-derivative of the potential for $z = 0$, we get:

$$v_\phi = \sqrt{R\left(\frac{\partial\Phi}{\partial R}\right)_{z=0}} \tag{64}$$

We show in the next figure the rotation curve for the Milky Way up to a distance of 12 kpc from the Galactic center.

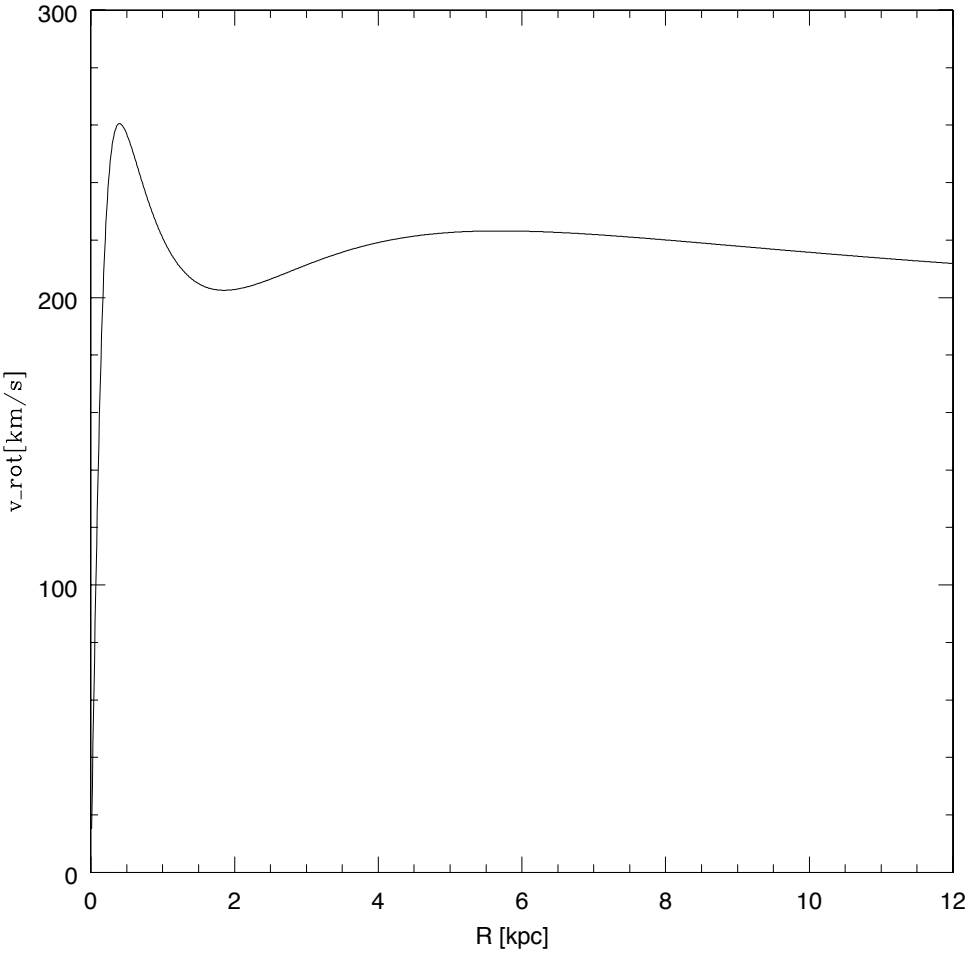

Figure 6: Rotation curve in the Galactic potential

.

In the last section we dealt with the velocity acquired by the center of mass of the system because of the SN explosion. This velocity will then add, with no preferred direction, to the Galactic rotation velocity: we will call the overall velocity as *space velocity*.

$$\mathbf{v}_{space} = \mathbf{v}_{sys} + \mathbf{v}_{\phi} \tag{65}$$

Typical rotational velocities in the Milky Way are of the order of few hundreds km/s (at $R = 8.0$ kpc, we get $v_\phi \sim 220$ km/s, which is the rotational velocity of the Sun). It's very interesting to note that this velocities are of the same order of magnitude of the binary orbital velocities; in this respect, we see how the common envelope, shrinking the orbital separation, increases the orbital speed: if orbital speeds were much higher than the typical velocities in the Milky Way potential, many systems would become unbound. In section 3.2.2, we have seen how the natal kick has just the same order of magnitude as the previously investigated velocities: a lucky circumstance that allows us to see LMXBs still bound in the Milky Way.

We now show some examples that have been used to test the integration code.
The orbit of the Sun in the Galactic potential is circular (fig. 7). If the sun received a kick in the Galactic plane, its orbit would turn into a *rosette orbit* (fig. 8). When a particle follows a rosette orbit, it oscillates between a minimum and maximum distance from the Galactic center while it revolves around the center, without the orbit being necessarily closed. This type of orbit is the most general trajectory for a particle with negative energy in a spherically symmetric potential, as the Galactic potential is provided that the particle is confined to the equatorial plane.

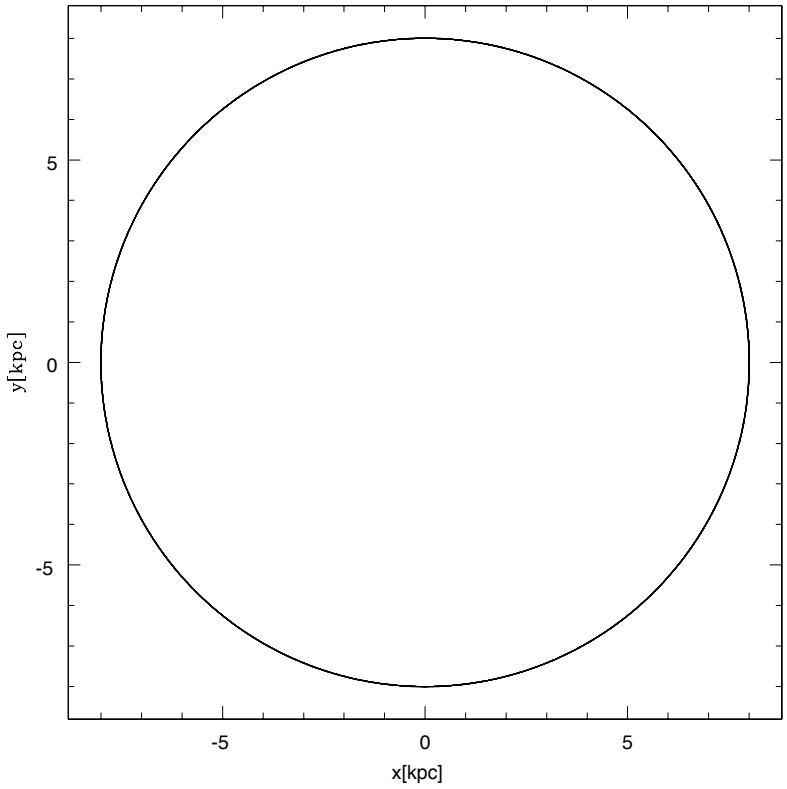

Figure 7: Sun trajectory in the Galactic potential. Integration for 5 solar orbit.

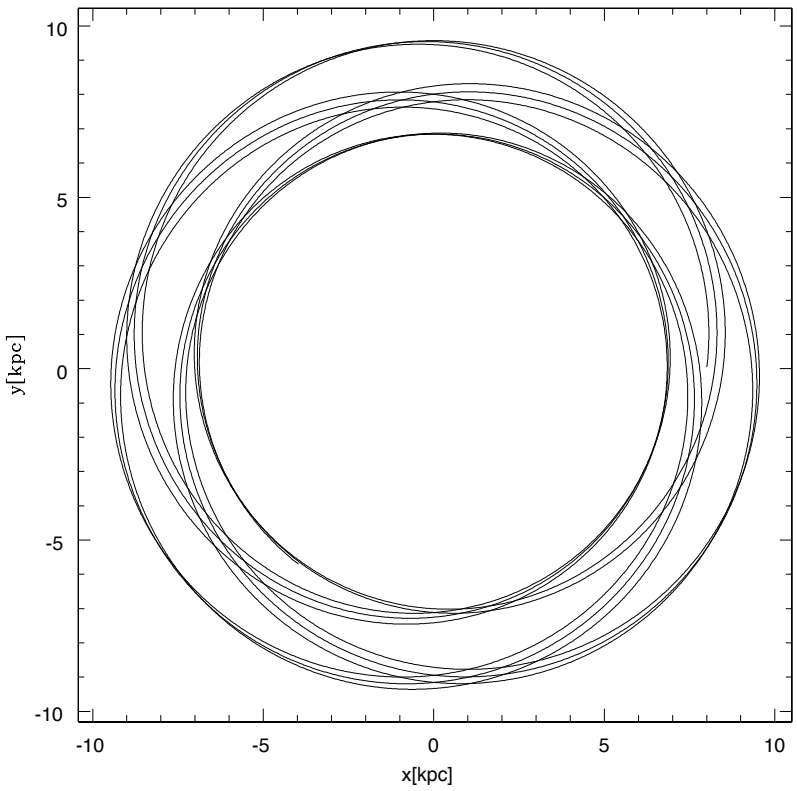

Figure 8: Sun that receives a kick of $\sim 50 km/s$ in the Galactic plane. Integration for 10 solar orbit.

The situation is more interesting for stars whose motions carry them out of the equatorial plane of the system. For example, if the Sun received a kick perpendicular to the Galactic plane, it would move out from the disk, and the projection of its orbit on the (R,z) plane would be the so-called *box orbit* (fig. 9). The box orbit clearly shows the oscillation of z between a minimum and a maximum value; projecting the motion over the equatorial plane we obtain the star revolving around the galactic center ([5]).

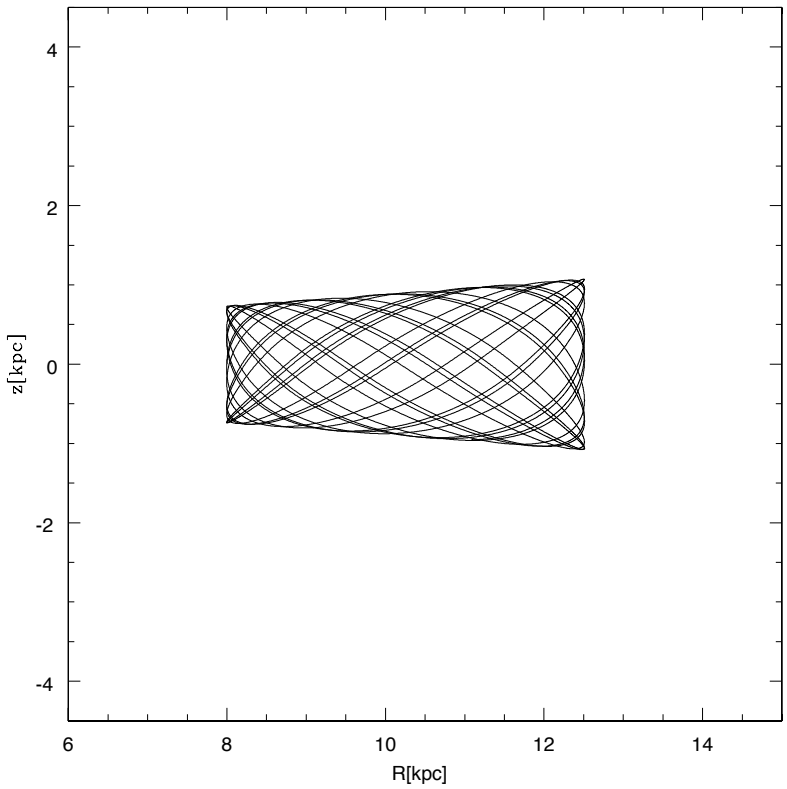

Figure 9: Sun that receives a kick of $\sim 50 km/s$ perpendicular to the galactic plane. Integration for 10 solar orbit.

We could wonder what would be the velocity that a perpendicular kick should have in order for the star to get to a certain observed z. This is computed via conservation of energy, neglecting the effect of Galactic rotation:

$$\frac{1}{2}{v_z}^2 + \Phi\left(R_0, 0\right) = \Phi\left(R_0, z_{max}\right) \tag{66}$$

In figure 10 we show the dependence of z_{max} from v_z: it's evident the tendency to escape for $v_z \gtrsim 250$ km/s. We would like to remind the reader that the escape speed is ~ 500 km/s at the solar neighborhood.

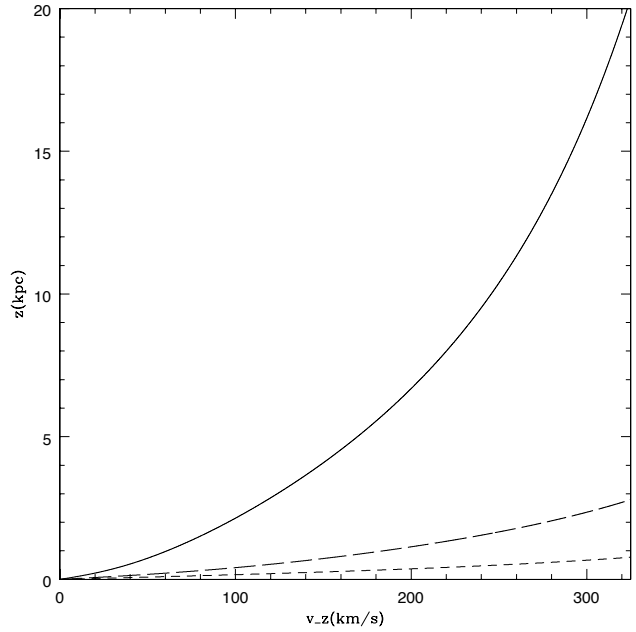

Figure 10: Maximum z reached by an object that receives a kick perpendicular to the Galactic plane. Solid line if for $R_0 = 8$ kpc; long-dash line is for $R_0 = 2.0$ kpc; short dash line is for $R_0 = 0.5$ kpc

5 Binary stellar evolution: what happens after the SN

After the formation of the BH, the binary system will then evolve in the Galactic potential up to the present day. The z-component of the space velocity determines its maximum distance from the Galactic plane.
Right after the BH formation up to the present day the system is subjected to effects that might shrink the post-SN orbital separation, such as tidal interactions and gravitational wave emission.
We now see the system thanks to its X-ray emission: mass transfer is currently due to the non-compact star expansion during the red-giant phase. At this stage, mass transfer happens to be from the less massive to the more massive one. Unlike the previously type of mass transfer, this time the orbital separation is caused to increase. Referring to equation (19) and assuming that the mass transfer is *conservative* (this means that both the mass and the orbital angular momentum are conserved), we get to:

$$\frac{\dot{a}}{a} = 2\frac{\dot{M}_2}{M_2}\,(q-1) \tag{67}$$

Since the mass ratio is in this case less than 1, we see that the time derivative of the orbital separation is positive. Consequently, the Roche radius gets larger. Mass transfer will start again when the star overflows its Roche lobe again thanks to its evolutionary expansion. Because of the low mass of the donor star, its nuclear timescale is long and accretion can go on for hundreds of millions years.

6 Observed systems: 16 BH candidates in LMXBs

Our Galaxy contains 23 black-hole candidates in binaries, of which 16 are found in LMXBs. For all of these 16 candidates, distances are known. Referring to Orosz 2003 ([23]) and to Örosz 2010 ([24]), we present in the following table some of the observational properties of the 16 BH-LMXBs: the distance projected on the Galactic plane R, the height above he Galactic plane z, the mass function *f(M)*, the mass ratio $q = M_2/M_1$, the inclination of the orbital plane with respect to the line of sight i and constraint on the mass of the black hole M_2. (We have taken the central values of the error bars in writing down R and z).

Object	R	z	f(M)	q	i	M_{bh}
2	3.92	0.70	0.25±0.01	0.25-0.31	20.7±1.5	9.4±1.0
3	5.0	-0.14	7.73±0.40	0.0-0.040	74.7±3.8	9.1±0.6
4	4.98	0.13	2.73±0.09	0.37-0.42	70.2±1.9	6.3±0.27
5	3.25	-0.67	5.8±0.5	0.0-0.4	-	-
6	2.14	-0.82	3.13±0.13	0.42-0.45	75±2	7.1±0.3
7	6.62	-0.03	9.5±3.0	0.025-0.091	66±2	-
8	7.65	-0.09	6.08±0.06	0.056-0.063	55±4	12±2
9	9.91	-0.41	1.19±0.02	0.076-0.31	-	-
10	8.92	-0.12	2.76±0.01	0.056-0.064	51.0±0.9	6.6±0.25
11	8.48	0.62	3.17±0.12	0.12-0.16	-	-
12	8.73	1.50	6.1±0.3	0.035-0.044	-	-
13	7.63	-0.73	3.01±0.15	0.11-0.21	-	-
14	5.71	-0.15	3.01±0.15	0.11-0.21	-	-
15	0.55	1.36	4.86±0.13	0.0-0.053	-	-
16	7.23	1.20	7.4±1.1	-	-	-
17	7.21	-0.14	5.01±0.12	0.035-0.053	-	-

Table 3: Properties of 16 LMXBs. (For object names refer to table 2).

In order to convert galactic coordinate into cylindrical ones, we use:

$$x = d_\odot - d_\odot \cos b \cos l \tag{68}$$

$$y = d_\odot \cos b \sin l$$

$$R = \sqrt{x^2 + y^2}$$

$$z = d_\odot \sin b$$

where $d_\odot$ is the distance of the Sun from the Galactic center.
In figure 11 we show the (R,z distribution) of our systems. Interestingly, we find that some systems are still in the disk, while other are found far out from the Galactic plane (at $|z| \gtrsim 1kpc$). We also plot the (x, y) distribution for the observed systems (fig. 12), taking the Galactic center as the origin of the coordinate system. We notice that our sample lack sources that have $x > 2$ as their x-coordinate: one legitimate question is then

whether our sample is sufficiently representative of BH candidates in LMXBs. We leave this question for future developments.

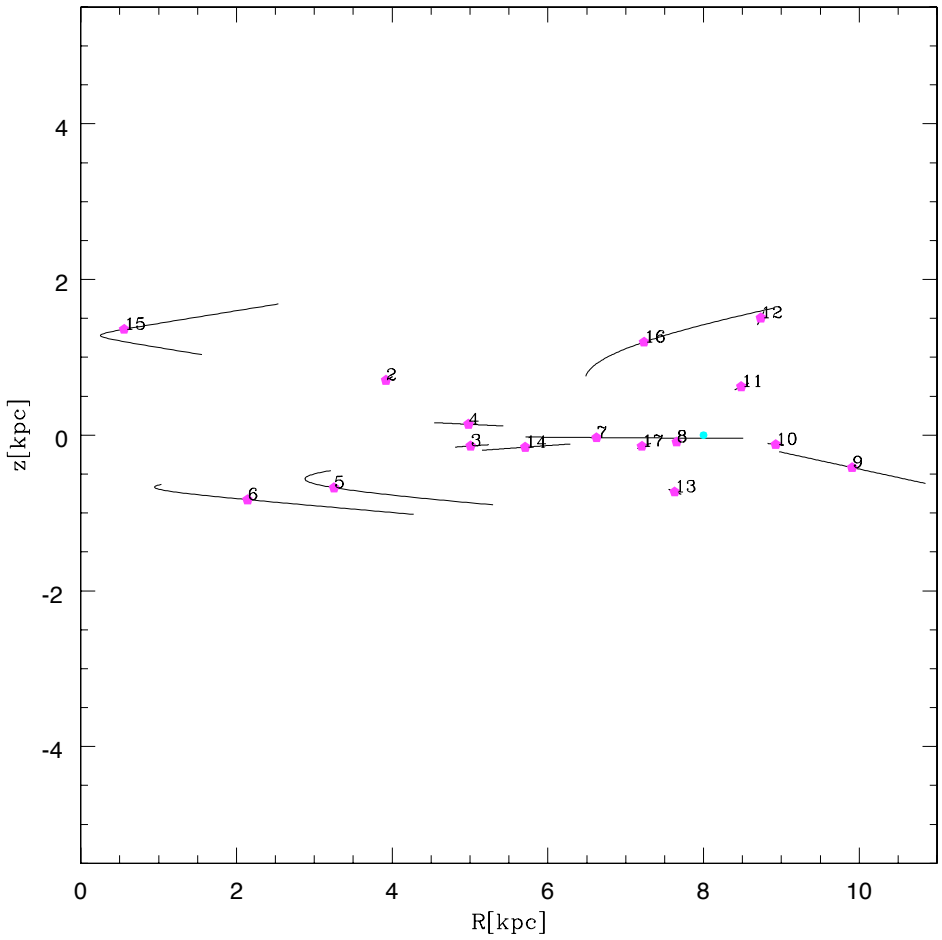

Figure 11: Galactic distribution in the (R,z) plane for the 16 systems. Lines corresponds to error bars due to the uncertainty in the distance. The blue dot corresponds to the Sun. The reference frame is centered at the Galactic center.

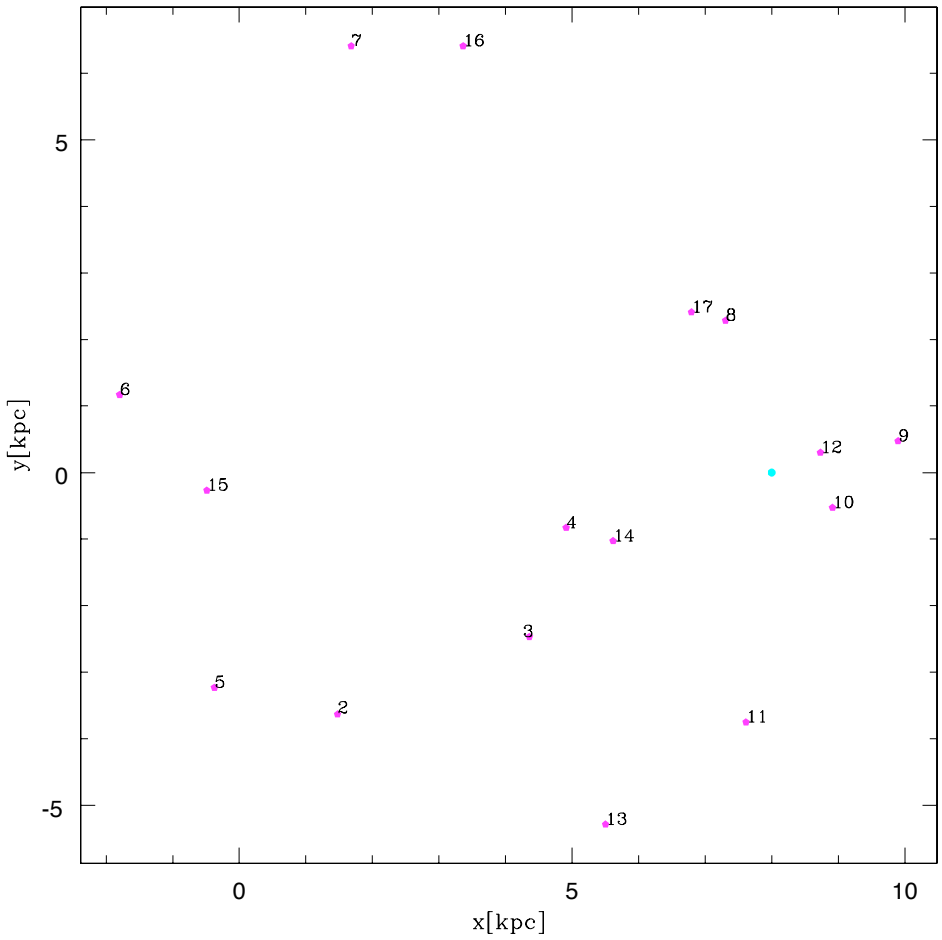

Figure 12: Galactic distribution in the (x,y) plane for the 16 systems. The blue dot corresponds to the Sun. The reference frame is centered at the Galactic center.

7 Study of the sources

We now aim at simulating the observed systems starting from some assumptions on the binary properties as well as on the initial conditions of the motion in the Galactic potential.

Before the supernova takes place, the typical orbital separation of the two stars is $\sim 10\ R_\odot$. This can be easily seen using equation (36), which gives the post-CE orbital separation in terms of the separation at the onset of the CE.
The system is assumed to be initially circular. In our first study, we computed the initial separation of the system assuming that the circularized post supernova orbital separation was coincident with the observed period (Nelemans 1999 [22]). We then realized that this assumption was far too simplistic. As a matter of fact, we cannot neglect the effects of the secular evolution on the binary properties, as well as of the mass transfer.
We guess the initial separation so that it fits both the radius of the Helium star ($R_{He} = 0.212(M_{He}/M_\odot)^{0.654} R_\odot$) (Tauris & van den Heuvel, 2003) and the radius of the unevolved companion star ($R_2 \sim \left(\frac{M}{M_\odot}\right)^{0.8} R_\odot$). We also require the Roche lobe of the non-evolved star to be bigger than the star radius: this is to prevent mass transfer from starting before the supernova explosion.
Information on the binary properties at the onset of the Roche lobe overflow are available for obj 12 (Fragos et al., 2009 [10]) and obj 4 (Willems et al., 2005 [31]). The orbital evolution of these two systems since the onset of the RLO has been followed through binary evolution codes, both in the case of conservative mass transfer and in the case of non conservative mass transfer. The result is a grid of evolutionary sequences for binaries in which a black hole is accreting mass from a Roche lobe-filling companion; each grid differs from another in the initial parameters chosen (mass of the black hole, mass of the donor and orbital separation). Then the best parameters are the ones that match the observed ones.
Thanks to this information, we put further constraints on the orbital separation. In case no natal kick is imparted to the compact object, it is possible to compute the post SN separation via equation (42), starting from our guess on the initial separation. We require its consistency with the orbital separation at the onset of the RLO: precisely, since it is legitimate to assume that secular evolution takes place, we ask that it is larger than the separation at the onset of RLO.
Regarding the components mass, we have to bear in mind that the masses inferred from the observational properties are different from the masses at the onset of the RLO, since mass transfer has already taken place. When mass transfer simulations are not available, we guess onset masses in order for them to be consistent with the observed ones. As concerning the mass of the Helium star, we require (in the case of symmetric supernova) that the mass loss is not larger than half of the initial mass.
As we said before, mass transfer changes the orbital separation. We can get an idea of the change in the simple hypothesis of conservative mass transfer. In this case, it is possible to compute the new orbital separation via conservation of angular momentum between the onset of the RLO and the current time:

$$\frac{a'}{a} = \left(\frac{M_1 M_2}{M_1' M_2'}\right)^2 \tag{69}$$

where primed variables refer to post mass-transfer values.
Nevertheless, this hypothesis fails when angular momentum is carried away from the sys-

tem (for example through the emission of jets).

After making sure that the binary orbital energy is still negative after the explosion, we proceed to the integration of the object in the Galactic potential, bearing in mind that the natal kick direction is uncorrelated with the orientation of the binary plane and that the system velocity that the object acquires because the explosion is uncorrelated with the rotation in the Galaxy.
We assume that our systems were born in the Galactic disk, taking z=0 as their initial distance from the Galactic plane. They orbit circularly around the Galactic centre at a distance $R \sim R_{obs}$ from it. We then apply to the black hole a kick drawn randomly from *Hansen & Phinney distribution* (and directed in a random direction with respect to the orbital velocity). The overall system velocity combines with the original velocity within the Galaxy, with no preferred directions. Since we are now observing the system within the Galaxy, its energy in the Galactic potential must be negative right after the explosion. Starting from these initial conditions, we integrate the equations of motion in the Galactic potential, for the main-sequence time of the companion star (it's important to stress that we assume stellar evolution to be not affected by the presence of the companion star). We consider 100 trajectories and for each trajectory we write down the positions (in cylindrical coordinates) for ten times drawn randomly from a uniform distribution over the whole integration time.
For all of the systems, we carry simulations both in the case of no natal kick imparted to the compact object and in the case of natal kick, and we present the simulated positions of the objects in the (R, z) plane.

7.1 XTEJ1118+480 (Object 12)

This object is observed high above the Galactic plane ($z \sim 1.5$) and has a period P=0.17 days (Mirabel et al., 2001 [20]). We kick the system at 7 kpc and we integrate its trajectory for $\sim 10^{10} years$.
For this object, information on the properties at the onset of the RLO are available (Fragos et al. (2009)).
The first simulation refers to the no natal kick case, while in second one Hansen & Phinney kick has been imparted to the black hole. The two simulations differ in the quantity of mass ejected in the supernova event, while the initial separation is unchanged. In the second one, the mass loss is lower compared to the first; as a consequence, the mass loss kick will be smaller: ∼24 km/s for a mass loss of 3 $M_\odot$ and $\sim$ 36 km/s for a mass loss of 5 $M_\odot$.
We present in table our guesses on the initial binary properties, as well as available information on the binary at the onset of the RLO and on the observed properties. In the first three columns, there are our guesses on the initial properties of the binary; in the middle one the properties of the binary when Roche lobe overflow sets in. When simulations of the mass transfer are not available, it is fair to guesses the RLO parameters so that they match both the initial ones and the observed ones. In the last column we have a gasp of how the system looks now. Most of the systems lack strong constraints on the inclination angle or on the mass of the companion star (see table 6): the mass of the black hole is generally constrained to be within an interval of uncertainty.

	initial parameters			parameters at the onset of RLO			observed parameters		
	M_{He} ($M_\odot$)	M_2 ($M_\odot$)	a_i ($R_\odot$)	$\widetilde{M_1}$ ($M_\odot$)	M_2 ($M_\odot$)	a_{rlo} ($R_\odot$)	M_{bh} ($M_\odot$)	M_2 ($M_\odot$)	a_{obs} ($R_\odot$)
Sim1	11	1	6	6	1	5	6.79	0.21	2.5
Sim2	9	1	6	6	1	5	6.79	0.21	2.5

Table 4: Selected properties for object 12, calculated to satisfy observational and RLO constraints

Figure 13: Object 12. (R,z) distribution for 100 trajectories. Top figure: no natal kick imparted to the black hole. Bottom figure: Hansen & Phinney natal kick.

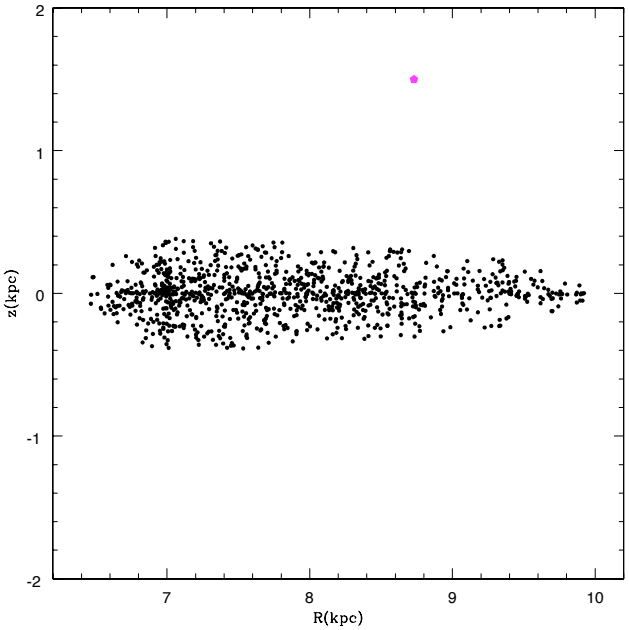

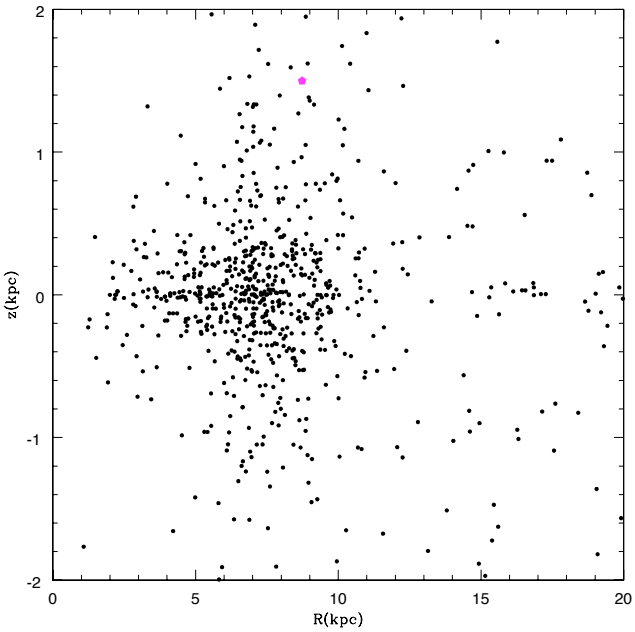

In the next figure we show an example of a trajectory for object 12; a Hansen & Phinney natal kick has been imparted to the black hole. We see that the observe position is well within the area covered by the box orbit.

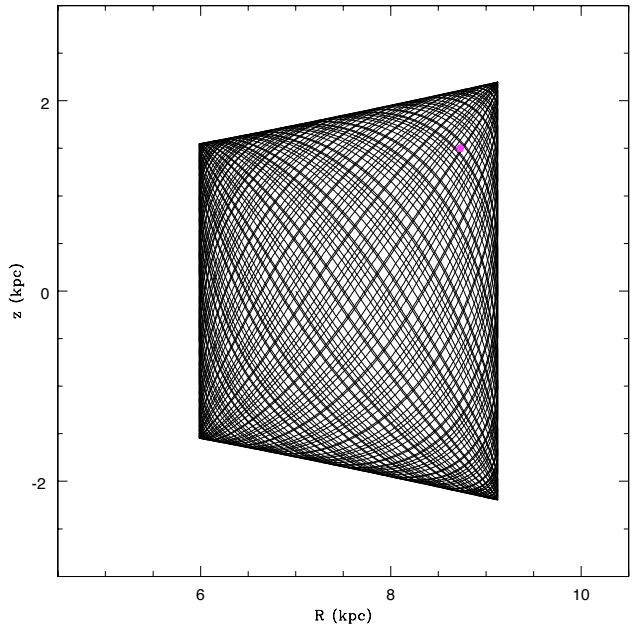

Figure 14: Example of a trajectory for Obj 12.

7.2 1705-250 (Obj 15)

This object is observed high above the Galactic plane ($z \sim 1.4$) and has a period P=0.52 days (Özel et al., 2010 [24]).
In figure 11 we can see that object 15 has a quite large error bars on the distance R from the Galactic center. We decide then to kick the system both from 2 kpc and from 0.5 kpc, and we integrate the trajectory for $\sim 3 \times 10^9 years$.
In table we show the binary properties, guessed and observed.

initial parameters			parameters at the onset of RLO			observed parameters		
M_{He}	M_2	a_i	$\widetilde{M_1}$	M_2	a_{rlo}	M_{bh}	M_2	a_{obs}
$(M_\odot)$	$(M_\odot)$	$(R_\odot)$	$(M_\odot)$	$(M_\odot)$	$(R_\odot)$	$(M_\odot)$	$(M_\odot)$	$(R_\odot)$
10	1.7	7	6.7	1.7	-	7	1.5	5.49

Table 5: Selected properties for object 15 calculated to satisfy observational constraints.

We plot the cumulative for the simulated z separating the natal kick case from the no natal kick case (see figure 15). We evidently see how the no natal kick scenario is not consistent with the observed position of the system, since the maximum z reached by the 100 simulated objects is well below the observed height from the Galactic plane.
From figure 15 it is also evident how a system kicked at $R = 0.5$ kpc reaches smaller z if compared to the same system kicked at $R = 2$ kpc. This is due to the dependence of the Galactic potential from R: the deeper we are in the potential well, the higher are the required velocities $v_{sys,z}$ to get to a fixed distance from the Galactic plane (see figure 10).
In figure 16 we show the (R,z) distribution of the simulated objects, both in the case of no natal kick and in case a Hansen & Phinney natal kick is imparted to the black hole. The initial distance from the Galactic center is taken to be 2 kpc.

Figure 15: Object 15, cumulative for z. Top figure: no natal kick imparted. Bottom figure: Hansen & Phinney natal kick. Solid line corresponds to $R(t_0) = 0.5kpc$; dotted line corresponds to $R(t_0) = 2kpc$.

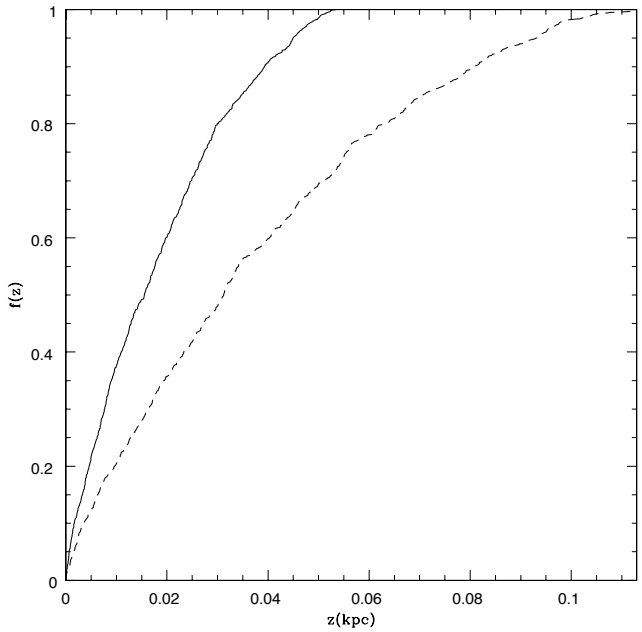

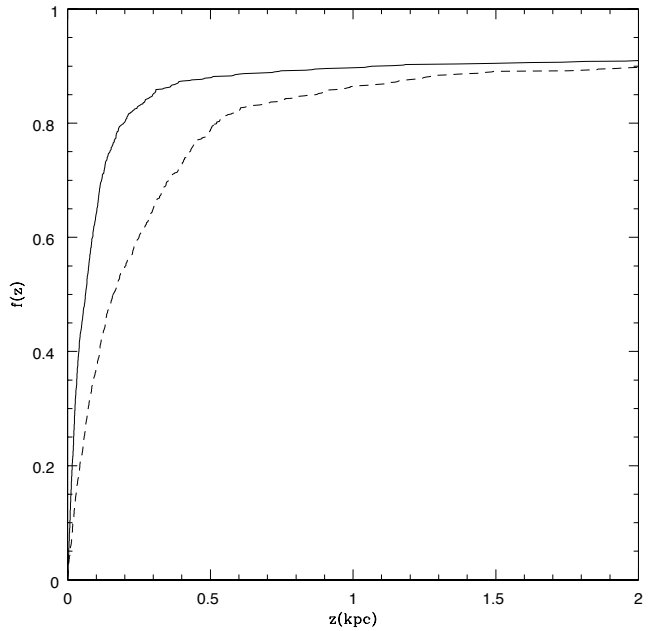

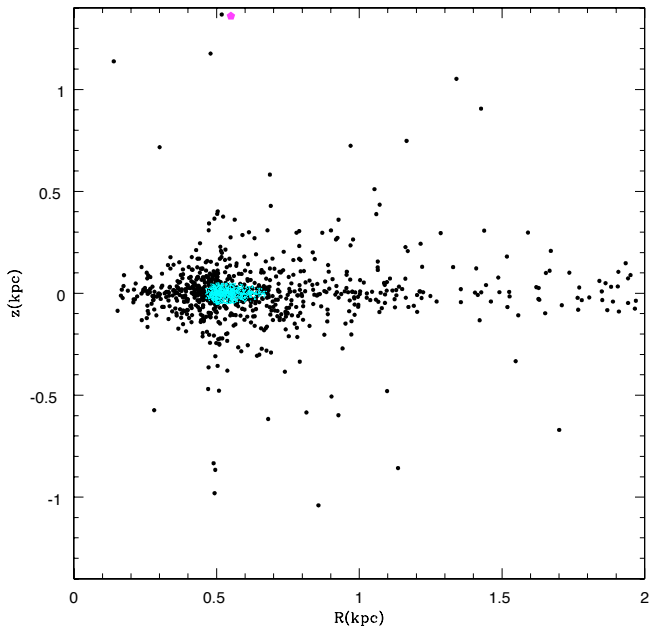

Figure 16: Object 15, (R, z) distribution for 100 trajectories. Black dots corresponds to Hansen & Phinney natal kick; blue dots correspond to the no natal kick case.

7.3 GRO1655-40 (object 4)

This object is almost coplanar ($z \sim 0.13$) and has a period P=2.62 days (Mirabel et al., 2002 [21]). This object is one of the few well-constrained between the 16 systems: strong limits on the mass function, on the inclination angle and on the mass of the black hole are available.
We kick the system at 5 kpc and we integrate its trajectory for $\sim 10^{10} years$. We performed simulations both in case of no natal kick and in case of natal kick.

initial parameters			parameters at the onset of RLO			observed parameters		
M_{He}	M_2	a_i	$\widetilde{M_1}$	M_2	a_{rlo}	M_{bh}	M_2	a_{obs}
$(M_\odot)$	$(M_\odot)$	$(R_\odot)$	$(M_\odot)$	$(M_\odot)$	$(R_\odot)$	$(M_\odot)$	$(M_\odot)$	$(R_\odot)$
10	2.5	10	6	2.5	15.5	6.3	2.3	16

Table 6: Selected properties for object 4 calculated to satisfy observational constraints

Figure 17: Object 4. Top figure: no natal kick imparted to the black hole. Bottom figure: Hansen & Phinney natal kick.

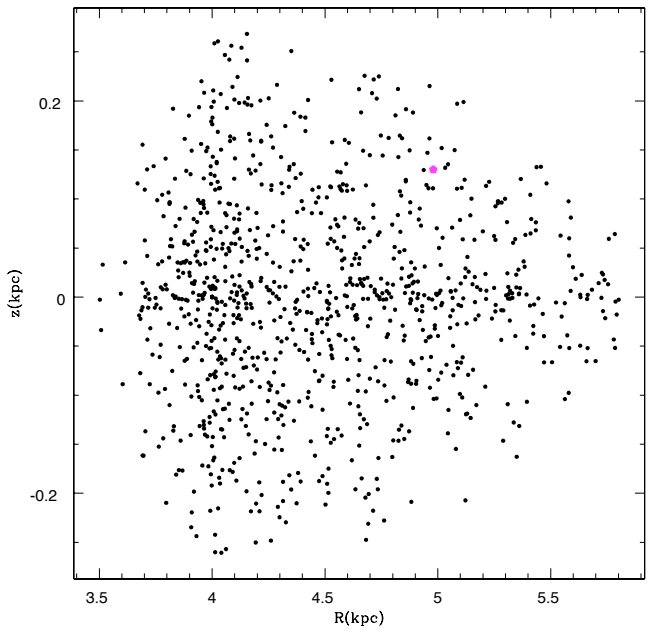

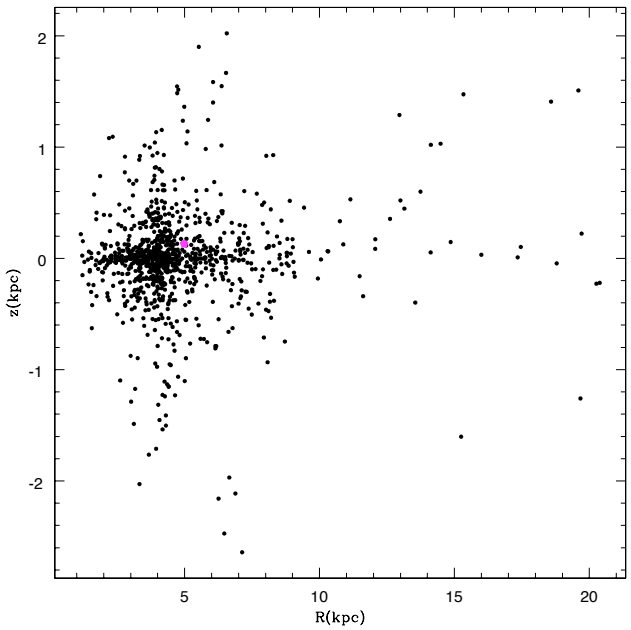

7.4 GRS1915+105 (Object 7)

This object is coplanar ($z \sim -0.03$) and has a period P=34 days (Dhawan et al., 2007 [8]). We kick the system at 6.7 kpc and we integrate its trajectory for $\sim 4 \times 10^9 years$. The two simulations, one for the no natal kick case and one for the natal kick case, differ in the guess on the initial orbital separation, while the mass loss is chosen to be equal. For fixed mass loss and initial masses, we know (see eq) that the square of the recoil velocity scales as the inverse of the orbital separation: the tighter the binary is, the bigger the recoil.

	initial parameters			parameters at the onset of RLO			observed parameters		
	M_{He} $(M_\odot)$	M_2 $(M_\odot)$	a_i $(R_\odot)$	$\widetilde{M_1}$ $(M_\odot)$	M_2 $(M_\odot)$	a_{rlo} $(R_\odot)$	M_{bh} $(M_\odot)$	M_2 $(M_\odot)$	a_{obs} $(R_\odot)$
Sim1	18	1.5	50	13.5	1.5	-	14	1.2	109
Sim2	18	1.5	80	13.5	1.5	-	14	1.2	109

Table 7: Selected properties for object 7 calculated to satisfy observational constraints

Figure 18: Object 7. Top figure: no natal kick imparted to the black hole. Bottom figure: Hansen & Phinney natal kick.

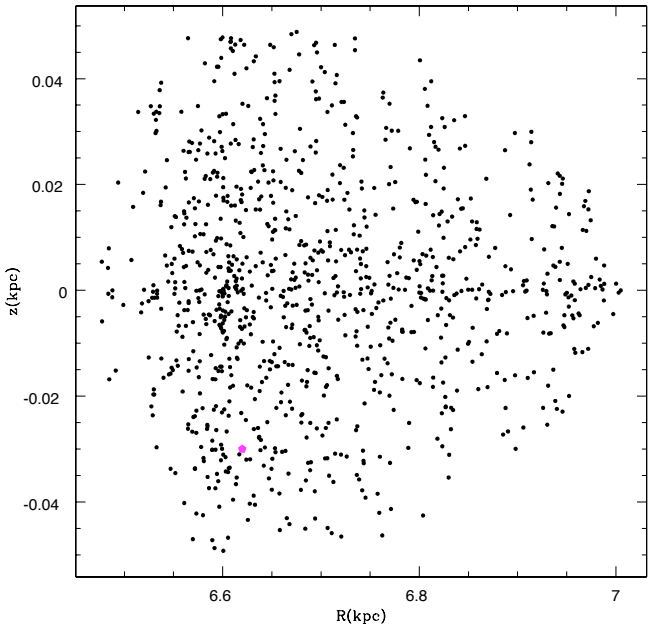

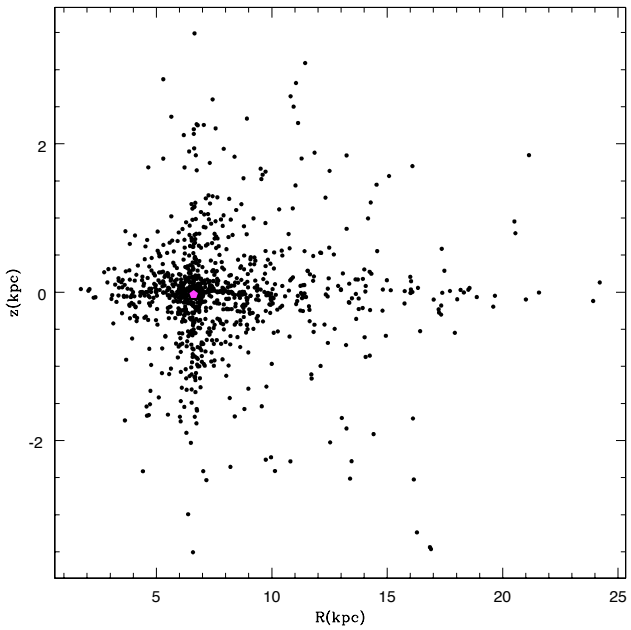

8 Discussion & Conclusion

From our simulations, we learn the difficulty in reproducing the high-z objects (in our case, obj 12 and 15) inside a no natal kick scenario. Instead, if the black hole receives a kick, the observed position is well inside the range of the simulated positions.

In the previously showed work, we treated each object singularly and independently. Each one has been kicked at a distance from the Galactic center comparable to the observed one, without taking into account the formation rate of binaries in our Galaxy.
From the surface density of stars $\Sigma(R) \sim \Sigma_0 e^{-R/R_d}$ (see appendix for details), we compute the number of stars located between R and $R + dR$ multiplying the mentioned density for the area $2\pi R dR$ of the ring. The radial density distribution is then f(R):

$$f(R)dR \propto Re^{-R/R_d}dR \tag{70}$$

where R is the distance from the Galactic center. In the next figure we show the radial density function:

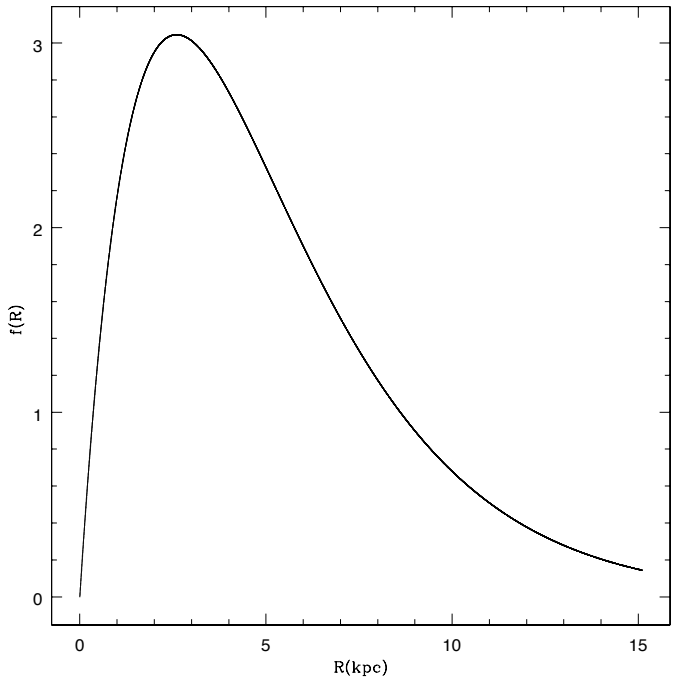

Figure 19: Radial density distribution of stars in the Galactic disk

We can legitimately assume that the radial distribution of binaries is proportional to the disk distribution of stars f(R) (Kolb et al., 2000 [16]). What's more, looking at the radial density distribution, it's evident how most massive stars are born with $R < 10$ kpc from the Galactic centre.

We build our population of 100 low mass X-ray binaries according to the previously showed radial distribution and constraining the initial distance form the Galactic center to be within $R = 10$ kpc, and then we kick each member of our population assuming z=0 as the initial distance of each system from the plane. We assign to each binary of our population the following typical orbital parameters: $M_1 = 11\ M_\odot$, $\widetilde{M_1} = 7.8\ M_\odot$, $M_2 = 1.5\ M_\odot$ and $a_i = 10\ R_\odot$.
One simulation is carried drawing kicks from the Hansen & Phinney distribution (ref. fig. 21), while in the second one the black hole doesn't suffer from a natal kick (see fig. 20).
We investigate also another possibility (ref. fig. 22). If we assume black holes and neutron stars to be born in the same way, that is, as previously seen, in core-collapse supernovae, we can legitimately suppose that the momentum they suffer from it is of the same order of magnitude. Due to their different masses, the natal kick will then be smaller for black holes:

$$v_{nk,bh} = \frac{M_{ns}}{M_{bh}} v_{nk,ns} \tag{71}$$

We will call this kick "*momentum conserving kick*" (MCK). For a neutron star mass of 1.4 $M_\odot$ and a black-hole mass of 7.8 $M_\odot$ (this is the pick of the observed black hole mass distribution in the Galaxy), black holes kicks are ~ 6 times lower. The correspondent natal kick distribution will then be obtained by shifting the neutron star kick distribution towards lower velocities.
For each of the 100 binaries, we compute the trajectory in the Galactic potential, carrying the integration for the main-sequence time of the companion star ($\sim 4 \times 10^9$ years), and we write down the R and z coordinates of the binary at 10 random times over the whole trajectory. We plot the correspondent (R,z) distribution for each scenario and compare it with the observed sample (see figure 11).

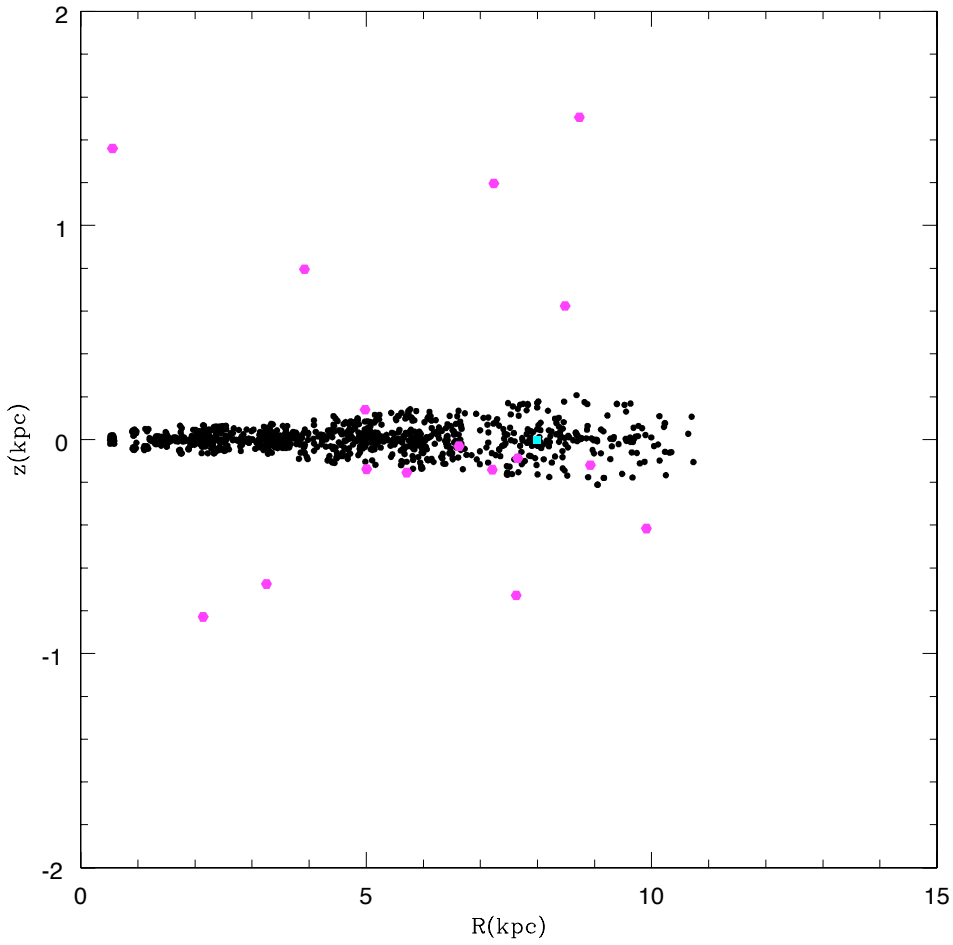

Figure 20: (R,z) distribution for a sample of 100 LMXBs. No Natal kick has been imparted.

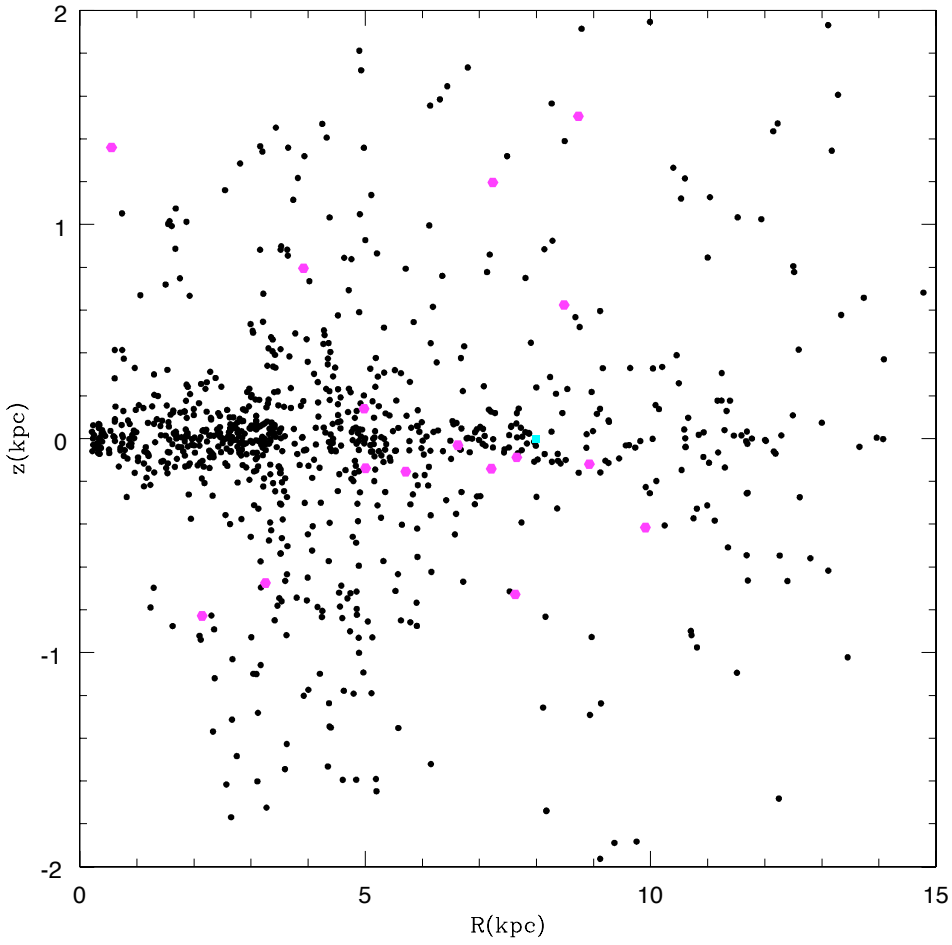

Figure 21: (R,z) distribution for a sample of 100 LMXBs. Kicks have been drawn from Hansen & Phinney distribution. 866/1000 points fall in the plotted R-z range.

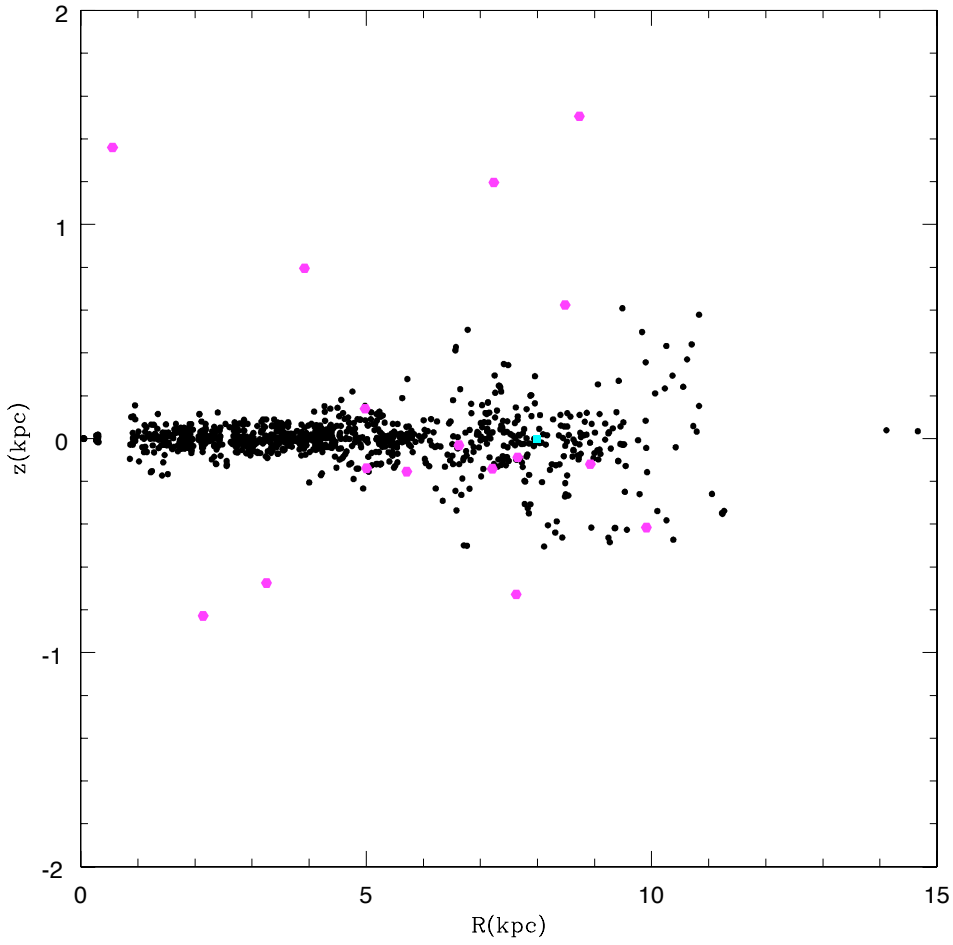

Figure 22: (R,z) distribution for a sample of 100 LMXBs. A momentum conserving kick has been imparted to the black hole. 997/1000 points fall in the plotted R-z range.

Plotting the correspondent cumulative for the z-values for all of the three scenarios and comparing it with the observed one (see figure 23), we see how all of the systems belonging to the no natal kick simulation have distance from the Galactic plane much lower than 1 kpc: the no-natal kick scenario evidently fails in reproducing the highest-z systems. The reduced kick also fails in reproducing the z-distribution of the observed systems.

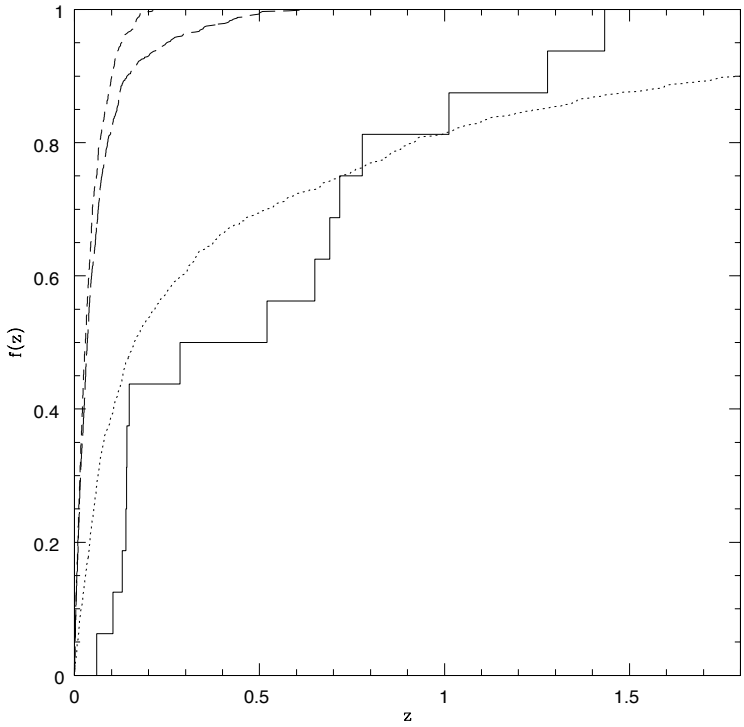

Figure 23: Cumulative for the z-values, both simulated and observed. Solid line refers to the observed distribution. Dotted line corresponds to H&P natal kick. Long-dash line corresponds to MCK and short-dash line corresponds to no natal kick.

One thing we would like to highlight is the fact that all our simulations for the different types of scenario contain much more systems further in towards the direction of the Galactic center: these systems are not observed in the Galaxy. On one hand, we don't actually see reasons for the presence of bias effects towards X-ray sources. On the other hand, the result is not surprising since we have decided to build our population assuming a surface density of stars centered around 3 kpc from the Galactic centre.
This issue lead us to re-evaluate the birth place of our systems: assuming a birth rate proportional to the surface density of stars is really consistent with the population of LMXBs? Or do we need to take spiral arms formation into account? We leave this question for further investigation.

We also compare the Hansen & Phinney natal kick scenario with a bimodal natal kick scenario. i.e. we associate to the newly formed compact object a kick randomly drawn from a distribution which is the superposition of two maxwellian distributions, one picked at lower velocities, the other one picked at higher velocities. We refer to Arzoumanian et al. 2002 ([1]) for our choice of the distribution:

$$f(v_{nk}) = 4\pi {v_{nk}}^2 \left\{ \left[w_1 \frac{1}{\left(2\pi\sigma_{v1}^2\right)^{3/2}} exp(-v_{nk}^2/2\sigma_{v1}^2) \right] + \left[(1-w_1) \frac{1}{\left(2\pi\sigma_{v2}^2\right)^{3/2}} exp(-v_{nk}^2)/2\sigma_{v_2}^2) \right] \right\} \tag{72}$$

where $\sigma_{v1} = 90$ km/s is the dispersion of the low-velocity component, $\sigma_{v2} = 500$ km/s is the dispersion of the high-velocity component and $w_1 = 0.4$ is the fraction of compact objects with a parent gaussian of width σ_{v1}.
We plot in figure the function, which show how the first peak is at ~ 100 km/s, while the second is at ~ 700 km/s:

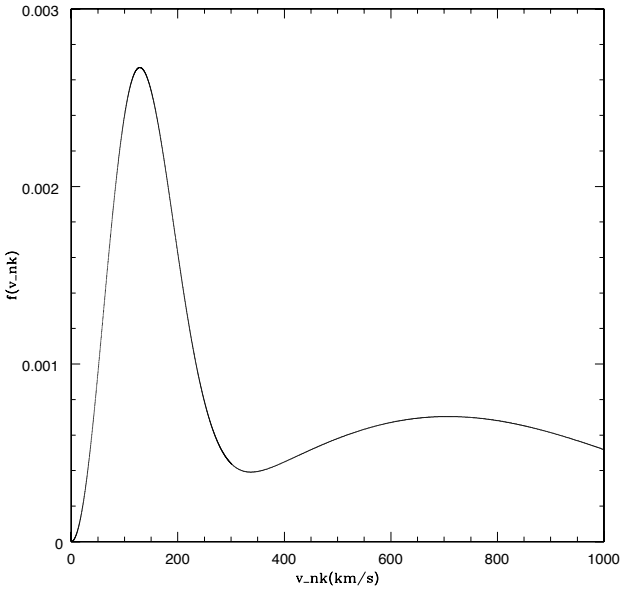

Figure 24: Bimodal distribution for the natal kick.

Comparing the cumulative for the associated z-values with the correspondent cumulative for the Hansen & Phinney scenario (see figure 26), we see that the a bimodal natal kick scenario has somewhat fewer systems with extreme value for z (i.e. with $z > 1.5$ kpc). Nevertheless, it's pretty evident from the shape of the cumulatives, that the cumulative associated with the Hansen & Phinney scenario better fits the observed one. This could be proved carrying a *Kolmogorov-Smirnov* test in order to compare our simulated samples with the observed one. Also, it's more difficult, within a bimodal kick scenario, to reproduce object 15, that is located further in over the Galactic center and at a large distance from the Galactic plane.

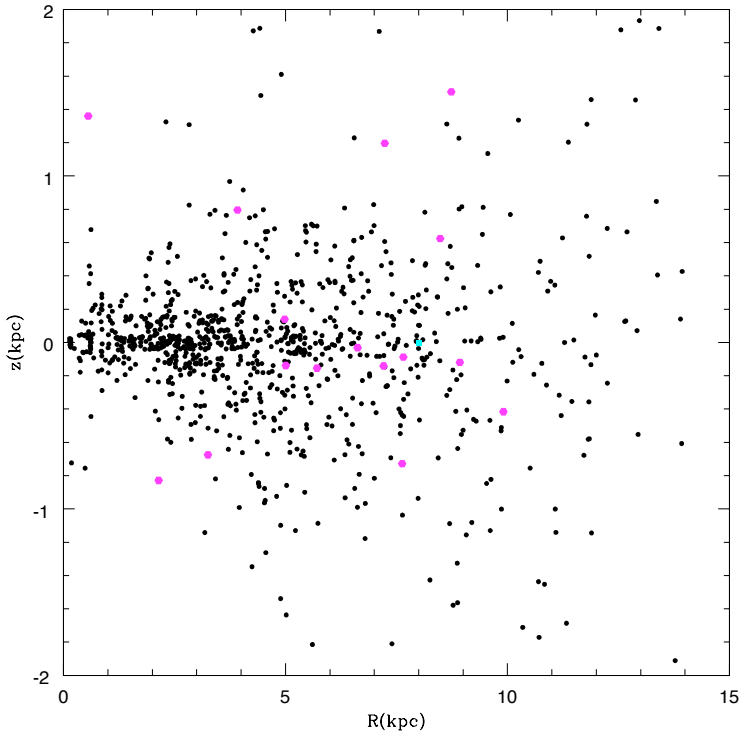

Figure 25: (R,z) distribution for a sample of 100 LMXBs. Kicks are drawn from a bimodal distribution. 960/1000 points fall in the plotted R-z range.

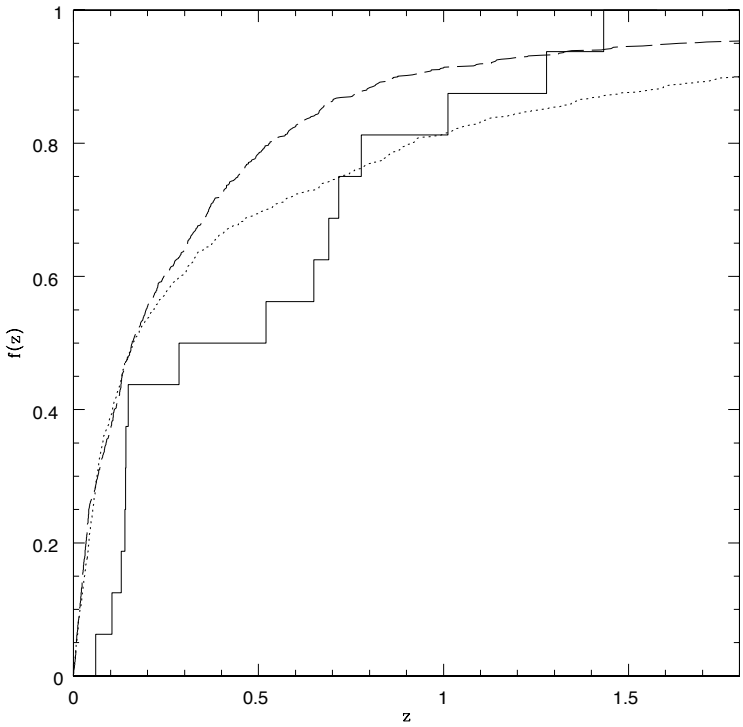

Figure 26: Cumulative for the z-values, both simulated and observed. Solid line refers to the observed distribution. Dotted line corresponds to H&P natal kick. Long-dash line corresponds to a bimodal distribution.

While carrying our simulations, we realized that populating our sample taking $z = 0$ as the initial distance from the Galactic plane for all of the systems, is not reasonable: we have to take into account the thickness of the disk. We can see this from our simulations: if we zoom in our simulated distributions closer to the plane, we see that most of our systems are almost in the plane. A more accurate choice is to consider a spread for the initial distance from the Galactic plane of the systems, for example drawing randomly from a uniform distribution between $z = -0.12$ kpc and $z = 0.12$ kpc (bearing in mind the the scale height of the thin disk, where most young stars are, is ~ 0.3 kpc [19]). We present the results in the following pictures. In figure 27 the (R,z) distribution of the simulated objects is shown: the kick that the black hole receives at birth is drawn from the Hansen & Phinney distribution and positions have been written dawn at uniform times over the trajectory. In the simulation correspondent to figure 28 kicks have been drawn from the Arzoumanian et al. distribution.
As previously seen, it is very difficult to make object 15 drawing kicks from a bimodal distribution: we need a Hansen & Phinney-like kick. This necessity becomes more evident if we plot the cumulative for z-values for the two types of scenario (see figure 29): again, the cumulative associated to the Hansen & Phinney scenario happens to fit better the observed data.

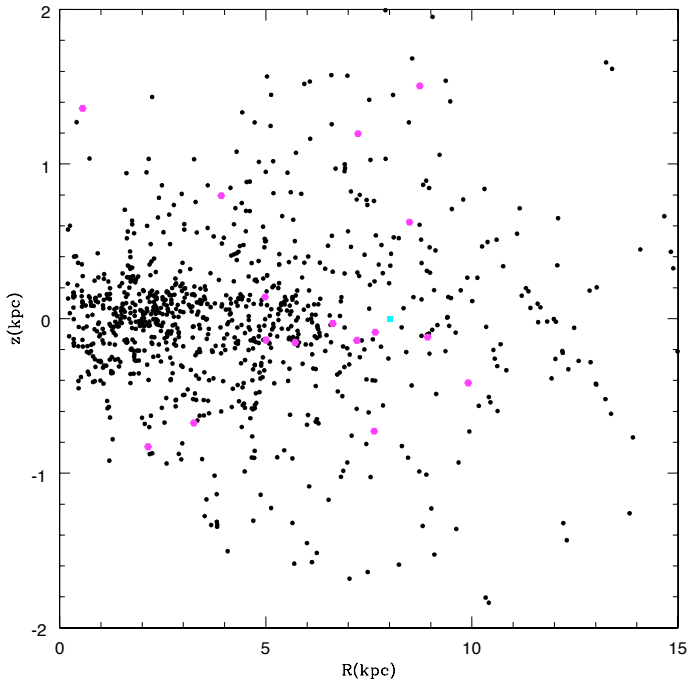

Figure 27: (R,z) distribution for a sample of 100 LMXBs. H&P kick has been imparted to the black hole and thickness of the disk has been taken into account.

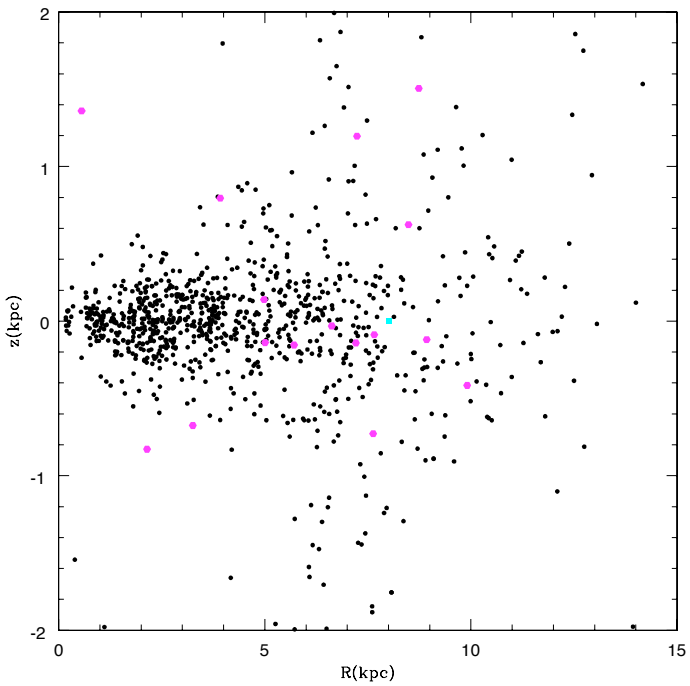

Figure 28: (R,z) distribution for a sample of 100 LMXBs. Kicks are drawn from a bimodal distribution and thickness of the disk has been taken into account.

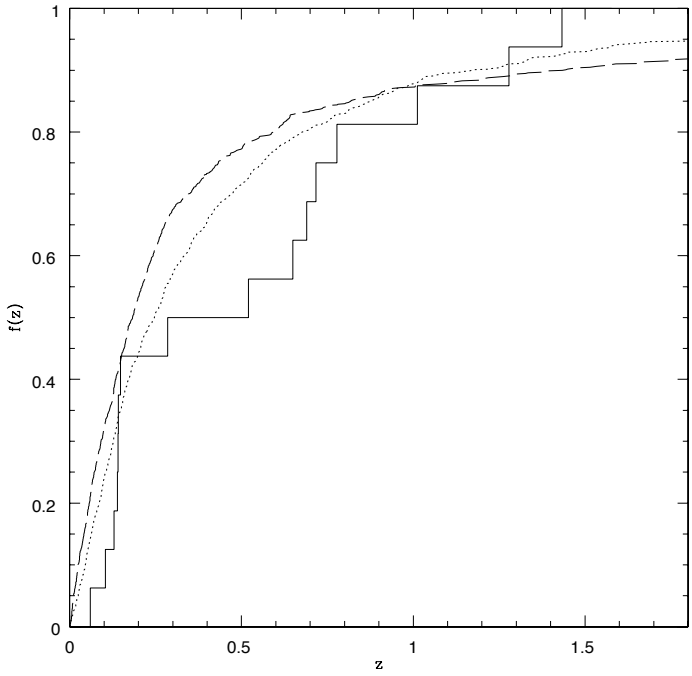

Figure 29: Cumulative for the z-values, both simulated and observed. Solid line refers to the observed distribution. Dotted line corresponds to H&P natal kick. Long-dash line corresponds to a bimodal distribution. The thickness of the disk has been taken into account.

Looking at the cumulative plot (see fig. 29), we see how, taking into account the thickness of the disk, we get for free the objects that have a distance from the Galactic plane $\lesssim 0.3$ kpc.

Considering the small observational sample and the simplicity of our model, the thing we can conclude is that a natal kick has to be imparted to the black hole for the simulated BH-LMXBs distribution to be consistent with the observed one. Also, it's very important to stress that this kick has to be of the same order of magnitude as neutron star kicks; as a matter of fact, from our simulations it is evident how the momentum conserving kick fails in reproducing the observed systems. Further analysis is needed in order to model correctly the natal kick distribution for black holes.

We want to acknowledge one important piece of information that it's missing in our work: the current space velocity of the system. A number of proper motions have been measured for Galactic X-ray binaries; when they are supplemented with measurements of the center of mass radial velocity as well as of the distance, the overall 3-dimensional kinematic can be reconstructed. All this wealth of information provide interesting insights into the formation history of the system. For instance, the backwards integration of the object in the Galaxy help to put constraints on the post supernova velocity of the system, which in turn helps to discriminate between the different formation scenario for black holes. This has been done by Fragos et al. (2009) for binary XTEj118+480: they conclude that a natal kick is indeed required for the formation of the system.
What's more, if an high peculiar velocity with respect to the Galactic rotation is detected, we can infer that the object is on a very eccentric orbit around the Galactic center. This can be due to a system velocity after the explosion almost in the plane of the Galaxy.

9 Appendix

9.1 The surface density of stars

The Milky way's disk is usually considered to have two major components: a thin disk and a thick disk (Gilmore & Reid, 1983 [12]). These are generally modelled as exponential:

$$\rho_d(R,z) = \frac{\Sigma_{d,0}}{2z_d} exp\left(-\frac{|z|}{z_d} - \frac{R}{R_d}\right) \tag{73}$$

where z_d is the scale height, R_d is the scale length and $\Sigma_{d,0}$ the central surface density.
The surface density of stars in the plane of the Galaxy is obtained evaluating the previous expression for $z = 0$:

$$\Sigma(R) \sim \Sigma_0 e^{-\frac{R}{R_d}} \tag{74}$$

The scale length of the thin disk, that has a younger population than the thick one, is $R_{d,thin} = 2.6 \pm 0.52 kpc$ (McMillan, 2011 [19]).
Integrating the surface density of stars over the whole disk, we get the radial density distribution:

$$f(R)dR = a_R R e^{(-R/R_d)} dR \tag{75}$$

where a_R is the normalization factor.

References

[1] Z. Arzoumanian, D. F. Chernoff, and J. M. Cordes. The velocity distribution of isolated radio pulsars. *The Astrophysical Journal*, 568(1):289, 2002.

[2] W. Baade and F. Zwicky. On Super-novae. *Proceedings of the National Academy of Science*, 20:254–259, May 1934.

[3] D. Bhattacharya and E. P. J. van den Heuvel. Formation and evolution of binary and millisecond radio pulsars. *Physics Reports*, 203:1–124, 1991.

[4] J. Binney and M. Merrifield. *Galactic Astronomy*. 1998.

[5] J. Binney and S. Tremaine. *Galactic dynamics*. 1987.

[6] N. Brandt and P. Podsiadlowski. The effects of high-velocity supernova kicks on the orbital properties and sky distributions of neutron-star binaries. *MNRAS*, 274:461–484, May 1995.

[7] M. B. Davies, A. R. King, and H. Ritter. A source of high-velocity white dwrfs. *Mon. Not. R. Astron. Soc.*

[8] V. Dhawan, I. F. Mirabel, and I. Rodrigues. Kinematics of black hole x-ray binary grs 1915+105. *The Astrophysical Journal*, 668(1):430, 2007.

[9] P. P. Eggleton. Approximations to the radii of Roche lobes. *ApJ*, 268:368–+, May 1983.

[10] T. Fragos, B. Willems, V. Kalogera, N. Ivanova, G. Rockefeller, C. L. Fryer, and P. A. Young. Understanding compact object formation and natal kicks. ii. the case of xtej1118 + 480. *The Astrophysical Journal*, 697(2):1057, 2009.

[11] J. Frank, A. King, and D. J. Raine. *Accretion Power in Astrophysics: Third Edition*. Feb. 2002.

[12] G. Gilmore and N. Reid. New light on faint stars. III - Galactic structure towards the South Pole and the Galactic thick disc. *MNRAS*, 202:1025–1047, Mar. 1983.

[13] H. Goldstein, C. Poole, and J. Safko. *Classical mechanics*. 2002.

[14] B. M. S. Hansen and E. S. Phinney. The pulsar kick velocity distribution. *MNRAS*, 291:569–+, Nov. 1997.

[15] P. G. Jonker and G. Nelemans. The distances to Galactic low-mass X-ray binaries: consequences for black hole luminosities and kicks. *MNRAS*, 354:355–366, Oct. 2004.

[16] U. Kolb, M. B. Davies, A. King, and H. Ritter. The violent past of Cygnus X-2. *MNRAS*, 317:438–446, Sept. 2000.

[17] L. D. Landau. Mechanics, Vol. I of Course on Theoretical Physics. *American Journal of Physics*, 40:1050–1051, July 1972.

[18] A. G. Lyne and D. R. Lorimer. High birth velocities of radio pulsars. *Nature*, 369:127–129, May 1994.

[19] P. J. McMillan. Mass models of the Milky Way. *ArXiv e-prints*, Feb. 2011.

[20] I. F. Mirabel, V. Dhawan, R. P. Mignani, I. Rodrigues, and F. Guglielmetti. A high-velocity black hole on a Galactic-halo orbit in the solar neighbourhood. *Nature*, 413:139–141, Sept. 2001.

[21] I. F. Mirabel, R. Mignani, I. Rodrigues, J. A. Combi, L. F. Rodríguez, and F. Guglielmetti. The runaway black hole GRO J1655-40. *Astronomy and Astrophysics*, 395:595–599, Nov. 2002.

[22] G. Nelemans, T. M. Tauris, and E. P. J. van den Heuvel. Constraints on mass ejection in black hole formation derived from black hole X-ray binaries. *Astronomy and Astrophysics*, 352:L87–L90, Dec. 1999.

[23] J. A. Orosz. Inventory of black hole binaries. In K. van der Hucht, A. Herrero, & C. Esteban, editor, *A Massive Star Odyssey: From Main Sequence to Supernova*, volume 212 of *IAU Symposium*, pages 365–+, 2003.

[24] F. Özel, D. Psaltis, R. Narayan, and J. E. McClintock. The Black Hole Mass Distribution in the Galaxy. *ApJ*, 725:1918–1927, Dec. 2010.

[25] B. Paczynski. A test of the galactic origin of gamma-ray bursts. *ApJ*, 348:485–494, Jan. 1990.

[26] P. Podsiadlowski, E. Pfahl, and S. Rappaport. Neutron-Star Birth Kicks. In F. A. Rasio & I. H. Stairs, editor, *Binary Radio Pulsars*, volume 328 of *Astronomical Society of the Pacific Conference Series*, pages 327–+, July 2005.

[27] C. E. Rhoades and R. Ruffini. Maximum Mass of a Neutron Star. *Physical Review Letters*, 32:324–327, Feb. 1974.

[28] S. Rosswog and M. Bruggen. *Introduction to High-Energy Astrophysics*. Apr. 2003.

[29] F. D. Seward and P. A. Charles. *Exploring the X-Ray Universe*. Nov. 1995.

[30] T. M. Tauris and E. van den Heuvel. Formation and Evolution of Compact Stellar X-ray Sources. *ArXiv Astrophysics e-prints*, Mar. 2003.

[31] B. Willems, M. Henninger, T. Levin, N. Ivanova, V. Kalogera, K. McGhee, F. X. Timmes, and C. L. Fryer. Understanding compact object formation and natal kicks. *The Astrophysical Journal*, 625(1):324, 2005.